

1 **Implications of the ongoing rock uplift in NW Himalayan interiors**

2 Saptarshi Dey¹, Rasmus Thiede², Arindam Biswas³, Naveen Chauhan⁴, Pritha Chakravarti¹, and
3 Vikrant Jain¹

4 ¹*Earth Science Discipline, IIT Gandhinagar, Gandhinagar-382355, India.*

5 ²*Institute of Geosciences, Christian Albrechts University of Kiel, Kiel-24118, Germany.*

6 ³*Department of Applied Geology, IIT-ISM Dhanbad, Jharkhand-826004, India.*

7 ⁴*Atomic Molecular and Optical Physics Division, Physical Research Laboratory, Ahmedabad.*

8 Corresponding author

9 Saptarshi Dey

10 saptarshi.dey@iitgn.ac.in

11
12 **Abstract**

13 The Lesser Himalaya exposed in the Kishtwar Window (KW) of the Kashmir Himalaya
14 exhibits rapid rock uplift and exhumation (~3 mm/yr) at least since the Late Miocene. However,
15 it has remained unclear if it is still actively-deforming. Here, we combine new field observations,
16 morphometric and structural analyses with dating of geomorphic markers to discuss the spatial
17 pattern of deformation across the window. We found two steep stream segments, one at the core
18 and the other along the western margin of the KW, which strongly suggest ongoing differential
19 uplift and may possibly be linked either to crustal ramps on the MHT or active surface-breaking
20 faults. High bedrock incision rates (> 3 mm/yr) on Holocene/Pleistocene timescales are deduced
21 from dated strath terraces along deeply-incised Chenab River valley. In contrast, farther

22 downstream on the hanging wall of the MCT, fluvial bedrock incision rates are lower (< 0.8
23 mm/yr) and are in the range of long-term exhumation rates. Bedrock incision rates largely
24 correlate with previously-published thermochronologic data. In summary, our study highlights a
25 structural and tectonic control on landscape evolution over millennial timescales.

26 **Keywords**

27 Steepness index; knickzone, rock strength; bedrock incision; Main Himalayan Thrust.

28

29 **1. Introduction**

30

31 Protracted convergence between the Indian and the Eurasian plate resulted into the
32 growth and evolution of the Himalayan orogen and temporal in-sequence formation of the
33 Southern Tibetan Detachment System (STDS), the Main Central Thrust (MCT), the Main
34 Boundary Thrust (MBT) and the Himalayan Frontal Thrust (HFT) towards the south (e.g., Yin
35 and Harrison, 2000; DiPietro and Pogue, 2004) (Supplementary Fig.B1). HFT defines the
36 southern termination of the Himalayan orogenic wedge and separates the orogen from the
37 undeformed foreland basin known as the Indo-Gangetic Plains. Seismic reflection profiles reveal
38 that all these fault-zones emerge from a low-angle basal decollement, the Main Himalayan
39 Thrust (MHT) forming the base of the Himalayan orogenic wedge (e.g., Ni and Barazangi, 1984;
40 Nabelek et al., 2009; Avouac et al., 2016), established in the late Miocene (Vannay et al., 2004).
41 Existence of MHT has further been elaborated in Himalayan cross-sections (e.g., Powers et al.,
42 1998; Decelles et al., 2001; Webb et al., 2011; Gavillot et al., 2018).

43 Lave and Avouac (2000) studied the late Pleistocene-Holocene shortening history of the
44 Central Nepal Himalaya where they showed the Holocene shortening is accommodated only
45 across the HFT. However, a large body of literature in the eastern, central and western Himalaya
46 favored that majority of the late Pleistocene-Holocene shortening is rather partitioned throughout
47 the Sub-Himalayan domain (morphotectonic segment in between the MBT and the MFT) and not
48 solely accommodated by the HFT (e.g., Wesnousky et al., 1999; Burgess et al., 2012; Thakur et
49 al., 2014; Mukherjee, 2015; Vassalo et al., 2015; Dey et al., 2016; Dey et al., 2018). The
50 statement above implies that the northerly thrusts, i.e., the MBT and the brittle faults exposed in
51 the vicinity of the southern margin of the Higher Himalaya, are considered inactive over
52 millennial timescales. However, in recent years, several studies which focused on the low-
53 Temperature thermochronologic data and thermal modeling of the interiors of the NW Himalaya
54 have raised questions on the statement above. The recent studies suggested that 1-3 mm/yr out of
55 the total Quaternary shortening has been accommodated in the north of the MBT as out-of-
56 sequence deformation (Thiede et al., 2004; Deeken et al., 2011; Thiede et al., 2017) or in form of
57 growth of the Lesser Himalayan Duplex (Gavillot et al., 2018) (Supplementary Fig. B2). For
58 faults within the hinterland of the Central Himalaya, the out-of-sequence deformation has been
59 explained by two end-member models. One of them favored the reactivation of the MCT (Wobus
60 et al., 2003), while the other tried to explain all changes along the southern margin of the Higher
61 Himalaya driven by enhanced rock uplift over a major ramp on the MHT (Bollinger et al., 2006;
62 Herman et al., 2010; Robert et al., 2009). Landscape evolution models, structural analysis and
63 thermochronologic data from the interior of the Himalaya favor that the Lesser Himalaya has
64 formed a duplex at the base of the southern Himalayan front by sustained internal deformation
65 since late Miocene (Decelles et al., 2001; Mitra et al., 2010; Robinson and Martin, 2014; Gavillot

66 et al., 2016). The growth of the duplex resulted into the uplift of the Higher Himalaya forming
67 the major orographic barrier of the orogen. The Kishtwar Window (KW) in the NW Himalaya
68 represents the northwestern termination of the Lesser Himalayan Duplex (LHD). While most of
69 the published cross-sections of the Himalayan orogen today recognize the duplex structures
70 within the Lesser Himalaya (Webb et al., 2011; Mitra et al., 2010; DeCelles et al., 2001; Gavillot
71 et al., 2018), little or no data are available on how the deformation is spatially as well as
72 temporally distributed and most importantly, whether a duplex is active over millennial
73 timescales.

74 The low-temperature thermochron study by Kumar et al., (1995) portrayed the first
75 orogen-perpendicular sampling traverse extending from the Kishtwar tectonic Window over the
76 Zaskar Range. More recent studies link the evolution of the KW to the growth of the Lesser
77 Himalayan Duplex structure (Gavillot et al., 2018), surrounded by the Miocene MCT shear zone
78 along the base of the High Himalayan Crystalline, locally named as the Kishtwar Thrust (KT)
79 (Ul Haq et al., 2019). Thermochronological constraints suggest higher rates of exhumation
80 within the window (3.2-3.6 mm/yr) with respect to the surroundings (~0.2 mm/yr) (Gavillot et
81 al., 2018), corroborating well with similar thermochron-based findings from the of the Kullu-
82 Rampur window along the Beas (Stübner et al., 2018) and Sutlej valley (Jain et al., 2000;
83 Vannay et al., 2004; Thiede et al., 2004) over the Quaternary timescale. No evidence exists
84 whether the hinterland of the Kashmir Himalaya is tectonically-active over intermediate
85 timescales. Therefore, to understand the 10^3 - 10^4 -year timescale neotectonic evolution, we
86 combined geological field evidences, chronologically-constrained geomorphic markers and
87 morphometric analysis of potential study areas, such as the KW. The detailed structural
88 information of the window and the surroundings, previously-published thermochron data,

89 accessibility, well-preserved sediment archive, and recognizable geomorphic markers across the
90 Kishtwar Window makes it a potent location for our study.

91 In this study, we focus on the following long-standing questions on Himalayan
92 neotectonic evolution, which are-

93 1. Is there any ongoing neotectonic deformation in the interiors of the Kashmir
94 Himalaya?

95 2. Can we determine sub-surface structural variations and existence of surface-breaking
96 faults by analyzing terrain morphology?

97 3. Can we obtain new constraints on deformation over geomorphic timescales? Do
98 millennial-scale fluvial incision rates support long-term exhumation rates?

99 To address these questions, we adopted a combination of methods such as morphometric
100 analysis using high-resolution digital elevation models, field observation on rock type, structural
101 variations as well as rock strength data and, analysis of satellite images to assess the spatial
102 distribution of the late Quaternary deformation of the KW and surroundings (Fig.1). We aimed to
103 evaluate the role of active tectonics and geometric variations in the basal decollement in shaping
104 the topography (Fig.1). We used basinwide steepness indices and specific stream power as a
105 proxy of fluvial incision. And, lastly but most importantly, we calculated the fluvial bedrock
106 incision rates by using depositional ages of aggraded sediments along Chenab River. In this
107 study, we show that the regional distribution of topographic growth is concentrated in the core of
108 the window and along the western margin of the window. Our new estimates on the bedrock
109 incision rate agree with Quaternary exhumation rates from the KW, which could mean consistent
110 active growth of the Kishtwar Window over million-year to millennial timescales. Although the

111 observed topographic and morphometric pattern indicate a structural/tectonic control on
112 topographic evolution, with the available data we are not able to resolve whether it is caused by
113 passive translation on the MHT or by active surface-breaking faulting within the duplex.

114

115 **2. Geological background**

116 Regionally balanced cross-sections (DiPietro and Pogue, 2004; Searle et al., 2007;
117 Gavillot et al., 2018) suggest that the Himalayan wedge is bounded at the base by décollement,
118 named the MHT and all regionally-extensive surface-breaking thrust systems are rooted to it.
119 The orogenic growth of the Himalaya resulted into an overall in-sequence development of the
120 orogen-scale fault systems which broadly define the morphotectonic sectors of the orogen (Fig.
121 1b). Notable among those sectors, the Higher Himalaya is bordered by the MCT in the south and
122 is comprised of high-grade metasediments, Higher Himalayan Crystalline Sequence (HHCS) and
123 Ordovician granite intrusives (Fuchs, 1981; Steck, 2003; DiPietro and Pogue, 2004; Gavillot et
124 al., 2018). The Low-grade metasediments (quartzites, phyllites, schists, slates) of the Proterozoic
125 Lesser Himalayan sequence are exposed between the MCT in the north and MBT in the south.
126 The Lesser Himalayan domain is narrow (4-15 km) in the NW Himalaya except where it is
127 exposed in the form of tectonic windows (Kishtwar window, Kullu-Rampur window etc.) in the
128 western Himalaya (Steck, 2003). The Sub-Himalayan fold-and-thrust belt lying to the south of
129 the MBT is tectonically the most active sector since the late Quaternary (Gavillot, 2014; Vassallo
130 et al., 2015; Gavillot et al., 2018).

131 Near the southwest corner of our study area, Proterozoic low-grade Lesser Himalayan
132 metasediments are thrust over the Tertiary Sub-Himalayan sediments along the MBT (Wadia,

133 1934; Thakur, 1992). Near the Chenab region in the Kashmir Himalaya, Apatite U-Th/He ages
134 suggest that cooling and exhumation related to faulting along the MBT thrust sheet initiated
135 before $\sim 5 \pm 3$ Myr (Gavillot et al., 2018). Geomorphic data obtained across the MBT in Kashmir
136 Himalaya suggest that MBT has not been reactivated for the last 14-17 kyr (Vassallo et al.,
137 2015). In the Kashmir Himalaya, the Lesser Himalayan sequence (LHS) exposed between the
138 MBT and the MCT is characterized by a < 10 km-wide zone of sheared schists, slates, quartzites,
139 phyllites and Proterozoic intrusive granite bodies (Bhatia and Bhatia, 1973; Thakur, 1992; Steck,
140 2003). The LHS is bounded by the MCT shear zone in the hanging wall. The MCT hanging wall
141 forms highly deformed nappe exposing lower and higher Haimantas, which are related to the
142 Higher Himalayan Crystalline Sequence (HHCS) (Bhatia and Bhatia, 1973; Thakur, 1992; Yin
143 and Harrison, 2000; Searle et al., 2007; Gavillot et al., 2018). Nearly 40 km NE of the frontal
144 MCT shear zone, MCT fault zone is re-exposed as a klippe in the vicinity of KW is called the
145 Kishtwar Thrust (KT) (Ul Haq et al., 2019) (fig. 1). Within the KW, Lesser Himalayan
146 quartzites, low-grade mica schists and phyllites along with the granite intrusives are exposed
147 (Fuchs, 1975; Steck, 2003; DiPietro and Pogue, 2004; Yin, 2006; Gavillot et al., 2018).

148 **2.1. Structural architecture of the Kishtwar Window**

149 The sub-surface structural formation beneath the KW is not well-constrained. A recent
150 study by Gavillot et al., (2018) proposes that the KW exposes a stack of LHS nappes in form of
151 the commonly-known Lesser Himalayan Duplex (LH duplex), characteristic of the central
152 Himalaya (Decelles et al., 2001). They also propose the existence of two mid-crustal ramps
153 beneath the KW, viz., MCR-1 and MCR-2 (fig. 1b). Based on thermochronological constraints
154 from Kumar et al., (1995), Gavillot et al. (2018) proposed that the core of the window is
155 exhumed with rates 3.2-3.6 mm/yr during the Quaternary, at a higher rate when compared to the

156 surroundings (~0.2-0.4 mm/yr). However, earlier studies by Fuchs (1975) and Frank et al.,
157 (1995) provide different insights to the formation of the KW. Fuchs (1975) proposed the
158 existence of two nappes- a. the Chail Nappe and b. the Lower Crystalline Nappe. The Lower
159 Crystalline nappe is partially or completely included in the MCT (KT) shear zone and the Chail
160 nappe encompasses the core of the window (Stephenson et al., 2000). According to these studies,
161 the Chail nappe has been internally deformed by crustal buckling, tight isoclinal folding causing
162 repetition and thickening of the LH crust.

163 The Higher Himalayan sequence dips steeply away from the duplex (~65° towards west)
164 (Fig.1, 2a). The frontal horses of the LH duplex expose internally-folded greenschist facies
165 rocks. Although at the western margin of the duplex, the quartzites stand sub-vertically (Fig.2c),
166 the general dip amount reduces as we move from west to east for the next ~10-15 km up to the
167 core of the KW. Near the core of the KW, we observed highly-deformed (folded and multiply-
168 fractured) quartzite at the core of the KW (Fig.2d, 2e). We also observed deformed quartz veins
169 of at least two generations, as well as macroscopic white mica. Here, the Chenab River is also
170 very steep and narrow; the rock units are also steeply-dipping towards the east (~55-65°) and are
171 nearly isoclinal and strongly deformed at places (Fig.2f). Towards the eastern edge of the
172 window, however, the quartzites dip much gently towards the east (~20-30°) (Fig.1b), and much
173 lesser folding and faulting have been recognized in the field (Fig.2g).

174 **2.2.Valley morphology**

175 The broad, 'U-shaped' valley profile near the town of Padder at the eastern margin of the
176 KW is in contrast with the interior of the window (Fig.3a). At the core of the KW, the Chenab
177 River maintains a narrow channel width and a steep gradient (Fig.3b). The E-W traverse of the
178 Chenab River through the KW is devoid of any significant sediment storage. However, along the

179 N-S traverse parallel to the western margin of the KW, beneath the Kishtwar surface, ~150-170m
180 thick sedimentary deposits are transiently-stored over the steeply-dipping Higher Himalayan
181 bedrock (Fig.3c). The height of the Kishtwar surface from the Chenab River is ~450m, which
182 means ~280m of bedrock incision by the River since the formation of the Kishtwar surface.
183 Along the N-S traverse of the River, epigenetic gorges are formed as a result of the damming of
184 paleo-channel by the hillslope debris flow, followed by the establishment of a newer channel
185 path (Ouimet et al., 2008; Kothyari and Juyal, 2013). One example of such epigenetic gorge
186 formation near the town of Drabshalla is shown in Fig.3d. Downstream from the town of
187 Drabshalla, the River maintains narrow channel width (< 25 m) and flows through a gorge
188 having sub-vertical valley-walls (Fig.3e). The tributaries originating from the Higher Himalayan
189 domain form one major knickpoint close to the confluence with the trunk stream (Fig.3f). We
190 have identified at least three strath surface levels above the present-day river channel, viz., T1
191 (280 ± 5 m), T2 (170-175 m) and T3 ($\sim 120\pm 5$ m), respectively (Fig.3g). The first study on
192 sediment aggradation in the middle Chenab valley (transect from Kishtwar to Doda town) was
193 published by Norin (1926). He argued the sediment aggradation in and around the Kishtwar town
194 is largely contributed by fluvio-glacial sediments and the U-shaped valley morphology is a
195 marker of past glacial occupancy. In general, we agree with the findings of Norin (1926) and Ul
196 Haq et al., (2019) as we observe ~100m thick late Pleistocene fluvio-glacial sediment cover
197 unconformably overlying the Higher Himalayan bedrock, most likely to be paleo-strath surface
198 (Fig.4b). At the same time, we do not agree with the interpretation of surface-breaking faults
199 near Kishtwar town by Ul Haq et al. (2019). We inspected the proposed fault locations in detail
200 and didn't observe any evidence of large-scale fault movement, including offset, broken and
201 rotated clasts, fault gouges etc. on the proposed fault planes. There is only one evidence of a

202 deformed sand layer which shows tilting and offset (<1 m). Therefore, we may conclude that we
203 found no strong evidence of any large-scale surface-breaking faults. The fluvioglacial sediments
204 included alternate layers of pebble conglomerate and coarse-medium sand (Fig.4c). The pebbles
205 are moderately rounded and polished suggesting significant fluvial transport. Our field
206 observations suggest that the fluvioglacial sediments have been succeeded by a significant
207 volume of hillslope debris flow and paleo-landslide deposit (Fig.4c). The thickness of the debris-
208 flow deposits is variable. The hillslope debris units and landslide deposits contain mostly
209 massive, highly-angular, poorly-sorted quartzite clasts from the steep western margin of the KW.
210 The hillslope debris units also contain a few fine-grain sediment layers trapped in between two
211 coarse-grained debris layers (Fig.4e). The town of Kishtwar is situated on this debris flow
212 deposit.

213

214 **3. Methods of morphometric analysis and field data collection**

215

216 **3.1.Morphometry**

217 For conducting the morphometric analysis, we have used 12.5m ALOS-PALSAR DEM
218 data (high resolution terrain-corrected) (Fig.5a). This DEM data has lesser issues with artifacts
219 and noises than 30m SRTM data, which fails to capture the drainage network properly in areas
220 populated by narrow channel gorges. Topographic relief has been calculated using a 4km moving
221 window (Fig.5b) and the rainfall distribution pattern has been adapted from 12-year averaged
222 annual rainfall data (TRMM data: Bookhagen and Burbank, 2006) (Fig.5c).

223 **3.1.1. Drainage network extraction**

224 The drainage network and the longitudinal stream profiles were extracted using the
225 Topographic Analysis Kit toolbox (Forte and Whipple, 2019). An equivalent of 10-pixel
226 smoothing of the raw DEM data has been applied to remove noises from the DEM. The
227 longitudinal stream profile of the Chenab trunk stream was processed with the Topotoolbox
228 ‘Knickpointfinder’ tool (Schwanghart and Scherler, 2014). Several jumps/ kinks in the
229 longitudinal profile are seen and those are marked as knickpoints (Fig.6). A 30m tolerance
230 threshold was applied to extract only the major knickpoints.

231 **3.1.2. Basinwide normalized steepness indices**

232 Global observations across a broad spectrum of tectonic and climatic regimes have
233 revealed a power-law scaling between the local river gradient and upstream contributing area:

$$234 \quad S = k_s \cdot A^{-\theta} \quad (1)$$

235 where S is the stream gradient (m/m), k_s is the steepness index ($m^{2\theta}$), A is the upstream
236 drainage area (m^2), and θ is the concavity index (Flint, 1974; Whipple and Tucker, 1999).
237 Normalized steepness-index values (k_{sn}) are steepness indices calculated using a reference
238 concavity value (θ_{ref}), which is useful to compare steepness-indices of different river systems
239 (Wobus et al., 2006). We extracted the k_{sn} values in the study area using the ArcGIS and
240 MATLAB-supported Topographic Analysis Toolkit (Forte and Whipple, 2019) following the
241 procedure of Wobus et al. (2006). We performed an automated k_{sn} extraction using a critical area
242 of $10^6 m^2$ for assigning the channel head, a smoothing window of 500 m, a θ_{ref} of 0.45, and an
243 auto- k_{sn} window of 250 m for calculating k_{sn} values. The slope-breaks, known as the knickpoints
244 (sometimes referred to as knickzones if it is manifested by a series of rapids instead of a single
245 sharp break in profile), were allocated by comparing the change of slope along the distance-
246 elevation plot (Fig.6, 7a). Threshold ‘dz’ value (projected stream offset across a knickpoint) for

247 this study is 30m. Basinwide mean k_{sn} values are plotted using a 1000 km² threshold catchment
248 area (Fig. 5d).

249 Identification of the knickpoints/ knickzones and their relationship with the rock-types as
250 well as with existing structures are necessary to understand the causal mechanism of the
251 respective knickpoints/ knickzones. Knickpoints/(zones) can be generated by lithological,
252 tectonic and structural control. Lithological knickpoints are stationary and anchored at the
253 transition from the soft-to-hard substrate. The tectonic knickpoints originate at the active tectonic
254 boundary and migrate upstream with time. Structural variations, such as thrust fault ramp-flat
255 geometry may cause a quasistatic knickpoint at the transition of the flat-to-ramp of the fault. In
256 such cases, the ramp segment is characterized by higher steepness than the flat segment and at
257 times the ramp may be characterized by a sequence of rapids, forming a wide knickzone, instead
258 of a single knickpoint.

259 ***3.1.3. Channel Width***

260 Channel width is a parameter of assessment of lateral erosion/incision through bedrocks
261 of equivalent strength (Turowski, 2009). The channel width of the Chenab trunk stream from just
262 downstream of the MBT up to the eastern margin of the KW was derived by manual selection
263 and digitization of the channel banks using the Google Earth Digital Globe imagery
264 (<http://www.digitalglobe.com/>) of minimum 3.2 m spatial resolution. We used the shortest
265 distance between the two banks as the channel width. We rejected areas having unparallel
266 channel-banks as that would bias the result. We used a 50 m step between two consecutive points
267 for channel width determination. Twenty point-averaged channel width data along with elevation
268 of the riverbed is shown in Fig.7b.

269 ***3.1.4. Specific stream power (SSP) calculation***

270 Specific stream power has often been used as a proxy of fluvial incision or differential
271 uplift along the channel (Royden and Perron, 2013; Whipple and Tucker, 1999). Areas of higher
272 uplift/incision are characterized by transient increase in the specific stream power. Channel slope
273 and channel width data were used to analyse the corresponding changes in the specific stream
274 power (SSP) from upstream of the gorge area to the gorge reaches (Bagnold, 1966). The SSP (ω)
275 was estimated using the following equation –

$$276 \quad \omega = \gamma \cdot Q \cdot s / w \quad (\text{Eq. 1})$$

277 Where, γ - unit weight of water, Q – water discharge, s – energy slope considered
278 equivalent to the channel slope; w – channel width. SSP data from selected stretches are shown
279 in Table 1. Channel width has been adapted from method described in section 3.1.3. We assumed
280 a uniform discharge throughout the study area, as the TRMM data show insignificant variations
281 in mean annual rainfall (Bookhagen and Burbank, 2006) (Fig. 5c, 5e). We also assume a runoff
282 ratio of 1 as we don't have any independent measure or supportive data of runoff vs. water
283 percolation through the bedrock and sediment archive.

284

285 **3.2. Field data collection**

286 **3.2.1. Structural data**

287 We measured the strike and dip of the foliations and bedding planes of the Lesser and
288 Higher Himalayan rocks using the Freiberg clinometer compass. At least five measurements are
289 taken at every location and the average of them has been reported in Fig. 8a. Field photos in the
290 Fig.2 support observed variations in the structural styles.

291 **3.2.2. Rock strength data**

292 Recording rock strength data in the field is important to understand the role of variable
293 rock-type and rock-strength in changes in morphology. It provides us important insights on the
294 genesis of knickpoints whether they are lithologically-controlled or not. It also helps to
295 understand the variations in channel steepness across rocks of similar lithological strength. We
296 systematically measured the rock strength of the main geologic units using a hand-held rebound
297 hammer. Repeated measurements (8-10 measurements at each of the 75 locations throughout the
298 study area) were conducted to measure the variability of rock-strength within the main lithologic
299 units (Fig. 7e). All the measurements were taken perpendicular to the bedding/ foliation plane,
300 and, no measurements are from wet surfaces or surfaces showing fractures. Each reading was
301 taken at least 0.5m apart from the previous one. To our benefit, most of the road-cut sections had
302 bedrock-exposures. Except restricted locations, e.g., dam-sites and military bases and outposts,
303 we were able to cover rest of the study area. To add to this, data taken from Higher Himalayan
304 intrusives close to the western margin of the KT are positively-biased as it represents readings
305 only from the leucosomatic layers. Our data from individual sites are smaller in number than
306 what is preferred for checking the statistical robustness of Schmidt hammer data (Niedzielski et
307 al., 2009). Therefore, we combined the data from all sites representing similar lithology and
308 portrayed the mean \pm standard deviation for the same. Field data on rock strength measurement
309 has been provided in Supplementary Table C1.

310 **3.3. Luminescence dating of transiently-stored sediments in and around Kishtwar**

311 Luminescence dating of Quaternary sediments is a globally accepted method for
312 constraining the timing of deposition of sediments across different depositional environments,
313 viz., Aeolian (Juyal et al., 2010), fluvial (Olley et al., 1998; Cunningham and Wallinga, 2012)
314 and glacial origin (Owen et al., 2002; Pant et al., 2006). In this study, we used luminescence

315 dating techniques to constrain depositional ages of several fluvioglacial and fluvial sand layers
316 exposed near the western margin of the KW and further downstream. Although there exists a few
317 persistent problems in luminescence dating of the Himalayan sediments (including poor
318 sensitivity of quartz and numerous cases of heterogeneous bleaching of the luminescence signal),
319 studies over the past couple of decades have also provided a good control on Himalayan
320 sedimentary chronology by using luminescence dating with quartz (Optically stimulated
321 luminescence, OSL) and feldspar (Infra-red stimulated luminescence, IRSL).

322 Samples K-07, K-08 and K-09 were collected from the medium-coarse sand beds of
323 fluvioglacial origin and have been dated with IRSL technique (Preusser, 2003). Standard IR-
324 protocol was used because the OSL signal was saturated and postIR-IR was showing instances of
325 heterogeneous bleaching. Samples K-02 and K-11 were taken from the fine sand-silt layers lying
326 above the debris-flow deposits and have been treated for OSL dating using double-SAR (single
327 aliquot regenerative) protocol (Roberts, 2007). Double-SAR protocol was used to surpass the
328 luminescence signal from tiny feldspar inclusions within individual quartz grains. Samples K-16
329 and K-17 taken above the T3 strath level, as well as the sample K-18, taken from above the T1
330 strath level were treated/ measured following the OSL double-SAR protocol. Samples K-01 and
331 K-06 taken above the bedrock strath near the town of Doda were also measured following OSL
332 double-SAR protocol. The aliquots were considered for equivalent dose (ED) estimation only if:
333 (i) recycling ratio was within 1 ± 0.1 , (ii) ED error was less than 20%, (iii) test dose error was less
334 than 10%, and (iv) recuperation was below 5% of the natural. Fading correction of the IRSL
335 samples K-07 and K-09 were done using conventional fading correction method (Huntley and
336 Lamothe, 2001). For samples showing over-dispersion (OD) $\leq 20\%$, central age model (CAM)
337 has been used for estimation of equivalent dose (D_e) (Bailey and Arnold, 2006) instead of

338 RMM-based De estimation as prescribed by Chauhan and Singhvi, (2011), useful for samples
339 having higher over dispersion (Table 2). For samples K-16 and K-17 having high OD value,
340 minimum age model (MAM) has been used. Details of sample preparation are provided in
341 supplement.

342 The dose rate was estimated using online software DRAC (Durcan et al., 2015) from the data of
343 Uranium (U), Thorium (Th) and Potassium (K) measured using ICP-MS and XRF (Table 2) in
344 IISER Kolkata. The estimation of moisture content was done by using the fractional difference
345 of saturated vs. unsaturated sample weight (Table 2).

346 **4. Results**

347

348 *4.1. Field observations and measurements*

349 The Chenab River has deeply incised the KW (Fig. 3b and 3e). The LHS rock units
350 exposed within the KW are mainly composed of fine-grain Quartzites and phyllites with
351 occasional schists in between. (Steck, 2003; Gavillot et al., 2018). The Lesser Himalaya has been
352 suggested to be an asymmetric antiformal stack with a steeper western flank (dip: 70°/west)
353 (Fig.2c). The KW is surrounded by rock units related to the Higher Himalayan high-grade
354 metasedimentary sequence, mainly garnet-bearing mica schists and gneisses. Higher Himalayan
355 rocks close to the western edge of the KW form a klippe with a southwest-verging MCT at its'
356 base. The KT, southern structural boundary of the window margin accommodating the
357 differential exhumation between window internal and surroundings, is expressed as highly
358 deformed sub-vertical shear bands.

359 **Along the traverse of the Chenab River through the KW and further downstream, two**
360 **prominent stretches along the Chenab River ~20 and ~25-30 km length are characterized by**

361 steep channel gradient associated with a large number of rapids (Fig.3b). These steep segments
362 are also characterized by a very narrow channel width (< 30m) (Fig.3b, 3e). The steepened
363 segments define knickzone (KZ) rather than a single knickpoint (KP). The knickzones KZ1 in
364 the trunk stream as well as in the tributaries are hosted over bedrock gorges. Although the
365 knickzone KZ2 pass through a series of old landslides (around Kishtwar town), the rapids have
366 all formed in bedrock channel. Therefore, neither KZ1 nor KZ2 appears to be related to
367 damming by recent landslides or other mass movements. The eastern margin of the KW is
368 characterized by a wide 'U-shaped' valley filled with thick sand layers and coarser fluvioglacial
369 sediments (Fig. 3a) where the Chenab River incises through this Late Pleistocene fill at present.

370 The rock strength data taken along the Chenab trunk stream portray large variations (R-
371 value ranging from 28 to 62) across different morphotectonic segments (Fig.7e). Within the KW,
372 Lesser Himalayan phyllites and schists have low R values (30-35); however, the low-strength
373 schists and phyllites are sparsely present and therefore, they are ignored while plotting the
374 regional rock strength values in Fig.7e. The dominant Lesser Himalayan quartzites in KW, as
375 well as the granitic intrusives in the eastern part of the KW, shows very high R values of 55-62
376 and 51-56 respectively (Fig. 7e). Compared to the high R values in the KW, the Higher
377 Himalayan metasediments show low strength (R: 35-45) till the point KP5 (Fig. 3b). However,
378 near the western margin of the KW, the migmatites of Higher Himalayan domain show high rock
379 strength (R value: 58 ± 3) (Fig.7e). The rock strength increases within the Haimanta Formation
380 (R: 44 ± 2) further downstream until it reaches the MCT shear zone at the southern boundary of
381 the Main Himalayan orogen. The R-value in the frontal Lesser Himalaya is moderate (R: 41 ± 2).

382 The Higher Himalayan sequence dips steeply away from the duplex ($\sim 65^\circ$ towards west)
383 (Fig.2a, 8a). The frontal nappes of the Lesser Himalaya expose internally-folded greenschist

384 facies rocks. Although at the western margin of the duplex, the quartzites stand sub-vertically,
385 the general dip amount reduces as we move from west to east for the next ~10-15 km (*Fig. 8*).
386 Near the core of the KW, we observed deformed quartz veins of at least two generations, as well
387 as macroscopic white mica. Near the core of the window, where the river is also very steep and
388 narrow, the rock units are also steeply-dipping towards the east (~60-65°) and are extremely
389 nearly isoclinal and vigorously deformed at places (*Fig.2d, 2e*). Towards the eastern edge of the
390 window, however, the quartzites dip much gently towards the east (~25-30°) and much lesser
391 folding and faulting have been recognized in the field.

392 The E-W traverse of the Chenab River is completely devoid of any sediment storage.
393 However, along the N-S traverse parallel to the western margin of the KW, ~150-170m thick
394 sedimentary deposits are transiently-stored over the steeply-dipping Higher Himalayan bedrock.
395 Norin (1926) argued the sediment aggradation in and around the Kishtwar town is largely
396 contributed by fluvioglacial sediments and the U-shaped valley morphology is a marker of past
397 glacial occupancy. We partially agree to the findings of Norin (1926) and Ul Haq et al., (2019) as
398 we observe >100m thick fluvioglacial sediment cover unconformably overlying the Higher
399 Himalayan bedrock along the N-S traverse of the Chenab River. The fluvioglacial sediments
400 included alternate layers of pebble conglomerate and coarse-medium sand. The pebbles are
401 moderately rounded and polished suggesting significant fluvial transport. Our field observations
402 suggest that the fluvioglacial sediments have been succeeded by a significant volume of hillslope
403 debris. The thickness of the debris-flow deposits is variable. The hillslope debris units contain
404 mostly coarse-grained, highly-angular, poorly-sorted quartzite clasts from the frontal horses of
405 the Lesser Himalayan Duplex. The town of Kishtwar is situated on this debris flow deposit
406 (*Fig.9*). Along the N-S traverse of the Chenab, we have observed at least two epigenetic gorges

407 lying along the main channel (Fig. 3d). The active channel has incised the Higher Himalayan
408 bedrock and formed strath surfaces. We have identified at least three strath surface levels above
409 the present-day river channel, viz., T1 (280±5 m), T2 (170-175 m) and T3 (~120±5 m),
410 respectively (Fig.3g, 10a).

411 **4.2. Results from morphometric analysis**

412 *4.2.1. Steep stream segments and associated knickpoints*

413 The longitudinal stream profile along the Chenab River does not portray a typical
414 adjusted concave-up profile across the Himalaya (Fig. 6). We observe breaks in slope and
415 concavity at several locations within a ~150 km traverse upstream from the MBT across the KW.
416 These breaks are defined as knickpoints. Starting from the eastern margin of the KW till the
417 MBT in the downstream, we identified at least six (6) discrete knickpoints in the river profile
418 (Fig. 6). Those are named KP1–KP6 according to their decreasing elevations. The upstream head
419 of KZ1 and KZ2 are marked as KP2 and KP3, respectively (Fig. 6).. The slope breaks define the
420 upstream reaches of the steep stream segments. The basinwide steepness indices span from ~30-
421 $>750 \text{ m}^{0.9}$ across the study area (Fig. 5d). We assigned a threshold value of $k_{sn}>550$ for the
422 steepest watersheds/ stream segments. Along the traverse, the major knickpoints are KP1
423 (~1770m), KP2 (~1700m), KP3 (~1150m) and KP5 (~800m) respectively (Fig.6). Two minor
424 knickpoints are there- KP4 (~1000m) and KP6 (~650m).

425 Already Nennewitz et al., (2018) had proposed a high basin-averaged k_{sn} value of > 300
426 in the KW. Here in this study, we worked with a much-detailed DEM and stream-specific k_{sn}
427 allocation (Fig.7d), as well as a basinwide steepness calculation. Our results corroborate with the
428 earlier findings, but, predict the zone of interest in greater detail. It is important to note that by

429 setting a higher tolerance level in the ‘knickpointfinder’ tool in Topotoolbox, we have managed
430 to remove the DEM artifacts from consideration (Schwanghart and Scherler, 2014).

431 **4.2.2. Channel width and valley morphology**

432 The channel width of the Chenab River is on average low (30-60m) within the core of the
433 KW (Fig. 3b, 7b), and the low channel width continues till the Chenab River flows N-S along the
434 western margin of the KW. However, there are a few exceptions; upstream from the knickpoint
435 KP1 in the Padder valley (in which the town of Padder is located), the channel widens (width
436 ~80-100m) and the channel gradient is low (Fig. 3a). The second instance of a wider channel is
437 seen upstream from knickpoint KP3, where there is a reservoir for the Dul-Hasti dam.
438 Downstream from KP3 within the Higher Himalaya, the channel width ranges from 50-70 m.
439 However, towards the lower stretches of the N-S traverse, the width is even lower (16-52m). The
440 river width increases to 100-200m as Chenab River takes a westward path thereafter. The
441 channel width increases beyond 300m until it leaves the crystalline rocks in the hanging wall of
442 the MCT and enters the Lesser Himalaya in the hanging wall of the MBT across the Baglihar
443 dam. Within the frontal LH, the channel width is again lowered (50-80 m).

444 **4.2.3. Changes in specific stream power (SSP)**

445 Discharge-normalized SSP data calculated from the upstream stretches and the
446 knickzones, KZ1 and KZ2 show major increase in SSP within the steep knickzones. The increase
447 in SSP from upstream to the knickzones KZ1 and KZ2 are 4.44 and 5.02 times, respectively
448 (Table 1). Such high increase in SSP is aided by steepening of channel gradient (Fig.7c) and
449 narrowing of channel bed (Fig.7b).

450 **4.3. Luminescence chronology**

451 The results for the luminescence chronology experiment are listed in Table 2. Samples
452 collected from the fluvio-glacial sediments overlain by debris flow deposit, namely as, K07, K08
453 and K09 yield IRSL ages of 104.5 ± 5.9 kyr, 114.4 ± 6.3 kyr, and 119.2 ± 6.8 kyr, respectively.
454 Fading corrections done for samples K07 and K09 yield the correction factors (g%) of 0.89 and
455 1.11 respectively. The sample K08 has not been treated for fading correction, but for easier
456 understanding, we have assumed a constant sedimentation rate between the samples K07 and
457 K09 and extrapolated the 'fading-corrected' age for K08. The oldest sample K09 (132 ± 7 kyr)
458 (fading-corrected IRSL age) is succeeded by samples K08 (126 ± 6 kyr) and K07 (113 ± 6 kyr)
459 respectively. The finer fraction of the hillslope debris overlying the fluvio-glacial deposits yield
460 OSL ages of 81.1 ± 4.6 kyr (K02) and 85 ± 5 kyr (K11) (Fig.6). OSL samples taken from sparsely-
461 preserved sediment layers above the T3 strath surface shows heterogeneous bleaching and hence
462 we provide a minimum age of 22.8 ± 2.1 kyr (sample K16) and 20.5 ± 1.0 kyr (sample K17). One
463 sample taken above T1 strath level is saturated and shows a minimum age of 52.1 ± 2.8 kyr
464 (sample K18) (Table 2). OSL samples K01 and K06 taken from sand layers sitting atop the
465 Higher Himalayan bedrock straths near the town of Doda portray depositional ages of 49.8 ± 2.9
466 kyr and 51.6 ± 2.4 kyr, respectively (Table 2).

467

468 **5. Discussions**

469

470 Analysis of morphometric parameters are widely used as indicators of active tectonics
471 and transient topography (Kirby and Whipple, 2012; Seeber and Gornitz, 1983). Many studies
472 have used morphometry as a proxy for understanding the spatial distribution of active
473 deformation across certain segments of the Himalayan front (Malik and Mohanty, 2007; van der

474 Beek et al., 2016; Nennewitz et al., 2018; Kaushal et al., 2017). More importantly, some studies
475 have integrated morphometric analysis with chronological constraints to assess the spatial and
476 temporal variability in deformation within the Sub-Himalaya (Lave and Avouac, 2000; Thakur et
477 al., 2014; Vassalo et al., 2015; Dey et al., 2016; Srivastava et al., 2018). All these studies have
478 demonstrated the applicability of morphometric indicators as an estimate of changes in uplift rate
479 or spatial variations of deformation across different landscapes.

480 Previously-published young Apatite fission-track cooling ages (~ 2-3 Myr) have been
481 interpreted as the result of rapid exhumation of the LH duplex over 10^6 -year timescale (Gavillot
482 et al., 2018). However, how and where the deformation is accommodated across the KW over the
483 10^3 - 10^5 -year timescale is unknown. In this section, we discuss the obtained morphometric and
484 fluvial characteristics of the studied region and compare these to existing models of deformation.
485 We also discuss how our new luminescence chronological estimates from the transiently-stored
486 sediment archive help us to constrain fluvial incision rates over Late Pleistocene- Holocene
487 timescale and put them in context to regional tectonic deformation models- 1. Mid-crustal ramp
488 model vs. 2. Out-of-sequence fault model.

489

490 **5.1. Knickpoints and their genesis**

491 Already Seeber and Gornitz (1983) had recognized along the Chenab River is
492 characterized by a zone of steep channel gradient in the vicinity of the KW. Nennewitz et al.,
493 (2017) demonstrated a strong correlation between steeped longitudinal river profiles and young
494 thermochronological cooling ages, suggesting recent focused rock uplift and rapid exhumation
495 along many major rivers draining the southern Himalayan front. Although, it is still an open
496 debate whether uplift and growth of the LH Duplex are triggered solely by slip over the crustal

497 ramp of the MHT or additional out-of-sequence surface-breaking faults are augmenting it
498 (Herman et al., 2010; Elliot et al., 2016; Whipple et al., 2016).

499 The longitudinal profile of the lower Chenab traverse (below ~2000 m above MSL) is
500 punctuated by two prominent stretches of knickpoint zones and several minor knickpoints related
501 to change of fluvial gradient (Fig.6). Below we will discuss the potential cause of formation of
502 those major knickpoints in the context of detailed field observation, of existing field-collected
503 structural and lithological data, geomorphic features, rock strength and channel width
504 information (Fig.7).

505 ***5.1.1. Lithologically-controlled knickpoints***

506 Our findings show that the The Himalayan traverse of the Chenab River is characterized
507 by large variations in substrate lithology and rock strength, which cause variations in the fluvial
508 erodibility and form knickpoints on the river profile (Fig.1, Fig.7e). An instance of soft-to-hard
509 substrate transition happens across the knickpoint KP1, lying downstream from the Padder
510 valley, at the eastern edge of the KW (Fig.2a). Across KP1, the river enters the over-deepened
511 LH bedrock gorge (R value > 50) after exiting the Padder valley filled with transiently-stored,
512 unconsolidated fluvio-glacial sediments (Fig. 3a). A similar soft-to-hard substrate transition is
513 observed upstream from the MCT shear zone. The corresponding knickpoint KP5 represents a
514 change in lithological formation from the sheared and deformed Higher Himalayan crystalline (R
515 value ~35-40) to deep-seated Haimantas (R value ~40-50). There is no field evidence, such as
516 fault splays or ramps, in support of KP5 to be a structurally-controlled one.

517 ***5.1.2. Tectonically-controlled knickpoints***

518 Compiling previously-published data on regional tectonogeomorphic attributes (Gavillot
519 et al., 2018) with detailed field documentation of structural styles and tectonic features; we

520 identified several stretches where variations in morphometric proxies indicate spatial variability
521 in rock uplift and faulting across the KW. We have found at least two instances where
522 knickzones are not related to change in substrate, nor are they artificially altered such as
523 constructed dam sites.

524 The knickzone KZ1 (upstream marked by KP2 ~1700 m above MSL) represents the
525 upstream reach of a steepened river-segment that represents a drop of ~420m of the Chenab
526 River across a run-length of ~15-20 km (Fig.8c). The upstream and downstream side of KP2 is
527 characterized by a change in dip of the LH bedrock foliation (Fig. 2f, 2g, 8) and channel width
528 (Fig. 7b). KP2 also reflects a change in the channel width (Fig. 7b). Interestingly, the steep
529 segment exhibits a narrower channel and particularly steep valley-walls through the core of the
530 KW. Near the end of the steep segment, intensely-deformed (folded and fractured) LH rocks are
531 exposed (Fig.2d, 2e). We infer two main possibilities for these field observations combined with
532 systematic changes of geomorphic characteristics – (1) it may be related to an active surface-
533 breaking out-of-sequence fault or (2) it may be an inactive fault that defines the floor-thrust of
534 one of the numerous proposed duplex nappes. On the contrary, the observed changes in the
535 geomorphic indices along with stretch of the knickzone KZ1 and observed increase in the
536 bedrock dip angle may well be explained by a ramp on the basal decollement. This explanation is
537 supported by the existence of mid-crustal ramps in the balanced cross-section from Gavillot et
538 al., (2018). However, the structural orientation of the rocks (Fig.8a) differ considerably than the
539 proposed LH duplex in Gavillot et al., (2008) raising questions about the duplex-model. Our
540 field observations are supported by previous studies by Fuchs (1975), Frank et al., (1995) and
541 Stephenson et al., (2000) who argued against duplexing of multiple thrust nappes and favoured
542 internal folding of Chail nappe to explain the tectonic growth and deformation pattern within the

543 **KW**. Therefore, we cannot clearly comment whether K1 represents a transition from flat to ramp
544 of the MHT or is it indeed an active out-of-sequence thrust-ramp.

545 On the other hand, the other knickpoint KP3 at the upstream-head of KZ2 nearly
546 coincides with the exposure of the KT (Fig.6). KP3 cannot be a lithologically-controlled
547 knickpoint as it reflects a hard-to-soft substrate transition from LH rocks (R value > 50) to HH
548 rocks (R value < 45) (Fig. 7e). We acknowledge that just across the point KP3, there are some
549 strong leucosomatic layers within the migmatites (R: 58 ± 3), but in general, the migmatites are
550 also brittle-deformed. The rock strength measurement was not done in the multiply-fractured
551 units as it would show inaccurate values. In the longitudinal profile, KP3 does not represent a
552 sharp slope break because the downstream segment runs parallel to main structures and KW-
553 boundary for ~25-30 km, including the KT. Therefore, we performed an orthogonal projection of
554 the E-W trending traverses of the Chenab River and estimated an orogen-perpendicular drop of
555 the Chenab across KZ2 (Fig. 8c). The truncated profile across KZ2 shows a drop of ~230m of
556 the channel across an orogen-perpendicular run-length of ~5 km. The orogen-parallel stretch of
557 the river exhibits narrow channel width (<30-35m) through moderately hard HH bedrock (R-
558 value: 35-45). The tributaries within this stretch form significant knickpoint at the confluence
559 with the trunk stream (Fig.3f). These field observations suggest recent rapid uplift of the western
560 margin of the KW. The observed differential uplift of the KW margin is possibly either related to
561 growth of the LH-duplex in the core of the window or by surface expression of another crustal
562 ramp emerging from the MHT (Fig.8d). Both the knickzones, KZ1 and KZ2 are the most-
563 prominent disturbance in the longitudinal profile of the Chenab River and are interpreted to
564 portray spatial distribution of differential uplift due to tectonic deformation..

565 **5.2. Temporal and spatial variation of fluvial incision across the KW**

566 Bedrock incision in the Himalaya is not a continuous process and is rather controlled by
567 temporal variations in sediment flux that usually dictates the thickness of the veneer above the
568 bedrock surfaces over which the rivers flow. Late Pleistocene-Holocene sediment transport
569 studies suggested an overall climatic control on sediment aggradation in the interiors of the
570 Himalayan orogen (e.g., Bookhagen et al., 2005; Scherler et al., 2015; Dey et al., 2016); where,
571 stronger climatic conditions may increase the sediment supply and prompt filling of a river
572 valley. Transiently-stored valley-fills are re-incised once the climate weakens. Often the re-
573 incision phases dissect the bedrock units and form strath surfaces. In Chenab valley, we have
574 documented several stages of valley-fills and fluvial strath surfaces.

575 ***5.2.1. Sediment aggradation in Chenab valley***

576 The Chenab valley records a net sediment aggradation and transient filling of entire
577 drainage network in the vicinity of the KW since the onset of the last glacial-interglacial cycle
578 (~130 kyr) till ~80 kyr. Fluvioglacial outwash sediments range from at least ~110-130 kyr,
579 whereas the hillslope debris ranges from ~90 to ~80 kyr (Table 2). The chronology of the
580 sediments is in agreement with the overall stratigraphic order of the sediments across the KW.
581 We observe net fluvial re-incision and formation of bedrock strath surfaces since ~80 kyr and
582 formation of epigenetic gorges(Fig.10).

583 ***5.2.2. Drainage re-organization and strath terrace formation along Chenab River***

584 Hillslope debris flow from the high-relief frontal horses of the Lesser Himalayan Duplex
585 overlies the fluvio-glacial sediments stored beneath the Kishtwar surface. We argue that the
586 hillslope debris are paleo-landslide deposits which intervened and dammed the paleo-drainage of
587 the Chenab River, which might have been flowing through an easterly path than now (Fig.9).
588 The Maru River, coming from the northwestern corner of our study area was also joining the

589 Chenab River at a different location (Fig.9). Our argument is supported by field observation of
590 thick silt-clay layer in the proposed paleo-valley of the Maru River (Fig.9a, 9c). OSL sample
591 (K18) from the silt-clay layer is saturated and hence only provide the minimum age of 52 ± 3 kyr.
592 We suggest that the hillslope sediment flux dammed the flow of the Chenab River and also
593 propagated through the aforesaid wind-gap of the Maru River. The decline in the depositional
594 energy has resulted into reduction of grain-size. Post-hillslope debris flow, the Chenab River also
595 diverted to a new path. The new path of the Chenab River upstream from the confluence with the
596 Maru River is defined by a very narrow channel flowing through the Higher Himalayan bedrock
597 gorge (Fig.7b). Downstream from the confluence, we are able to identify at least three levels of
598 strath terraces lying at heights of ~280-290m (T1), ~170m (T2) and ~120m (T3), respectively
599 (Fig.3g,10a). Our field observation suggests that the formation of the straths is at least ~52 kyr-
600 old. The luminescence chronology samples in this study belong to the ~150-170m-thick soft
601 sediments that are stored stratigraphically-up from the T1 strath level. Our field observations and
602 chronological estimates suggest that the renewed path of the Chenab River, must have been
603 formed post the hillslope debris flow ~80-90 kyr but before 52 kyr.

604 ***5.2.3. Knickpoint marking epigenetic gorge***

605 Epigenetic gorges are common geomorphic features in the high-mountain landscape
606 (Ouimet et al., 2008). Epigenetic gorges form when channels of a drainage system are transiently
607 buried by sediment aggradation and during subsequent re-incision, a new river channel, often
608 into the neighboring bedrock is incised. The N-S traverse of the Chenab River is largely affected
609 by hillslope sediment flux (paleo-landslides and debris flow) from the steep eastern flank. The
610 knickpoint KP4 situated near the village of Janwas, mark one such instance of epigenetic gorge

611 where the paleo-valley has been filled initially by fluvio-glacial sediments and the channel
612 abandonment was caused by landslides and hillslope debris flow prior to 80 kyr (Fig. 4b, 4c).

613

614 **5.3. Rapid bedrock incision along Chenab River on Late Pleistocene timescale**

615 Considering the rate of excavation of softer sediments to be at least an order of magnitude
616 higher than the rate of bedrock incision (Kothyari and Juyal, 2013; Sharma et al., 2016), we
617 calculated the minimum bedrock incision rate at the western margin of the KW, using the height
618 of the T1 strath ($\sim 280 \pm 5$ m) and the average age of the sediments from the Hillslope debris flow
619 deposit. It yields a minimum bedrock incision rate of ~ 3.1 - 3.5 mm/yr over the last 80-90 kyr.
620 Considering the saturated OSL sample from the paleo-valley, we estimated the maximum
621 bedrock incision since 52 kyr to be 5.1 - 5.5 mm/yr. Similarly, using the minimum age estimate of
622 the T3 terrace abandonment, we deduce a maximum bedrock incision rate of ~ 5.7 - 6.1 mm/yr
623 since ~ 21 kyr. However, further downstream, away from the KW, the average bedrock incision
624 rate derived from dated strath surfaces ($\sim 36 \pm 2$ m high from the Chenab River) near the town of
625 Doda is 0.7 ± 0.1 mm/yr (sample K01 and K06). We don't have bedrock incision rates from the
626 core and the eastern margin of the KW, as the core is devoid of sediment storage and the eastern
627 margin is filled with fluvio-glacial sediments and the river is incising the fill. These results
628 indicate that despite transient choking of the drainage network by sediments during times of
629 valley aggradation, the topography experienced high incision, when sediment coverage had been
630 completely penetrated and bedrock straths had been created post-renewal of the fluvial flow.

631

632 **5.4. Our new results in context with the previously-published data**

633 AFT-cooling ages by Kumar et al., (1995) showcased young cooling ages from the core
634 of the KW and its western margin (AFT ages: ~2-3 Myr) compared to the surroundings (AFT
635 age: 6-12 Myr). The calculated high exhumation rates proposed by Gavillot et al., (2018) are
636 based on using a geothermal gradient of 35-40°C/km in Dodson's equation assuming a 1-D
637 model (Dodson, 1973). Additional data and thermal modeling are needed across the KW to
638 constrain the exhumation rates from vertical transect. However, lateral similarities of the regional
639 topography and age patterns along the Sutlej area, Beas and Dhauladhar Range (Thiede et al.,
640 2017; Thiede et al., 2009; Stübner et al., 2018) have yielded similar exhumation rates in the
641 range of 2-3 mm/yr and are confirming obtained rates. **Long-term exhumation rates from the NW**
642 **Himalaya** agree well with findings of Nennewitz et al. (2018) who correlated the young
643 thermochron ages with high basinwide k_{sn} values suggesting high uplift rates over intermediate
644 to longer timescales. Although the geomorphic implications on landscape evolution provide
645 resolution at shorter timescales than the low-T thermochron studies, our field observations and
646 analysis support very well a protracted long-term uplift rates across the KW. Interestingly,
647 exhumation rates steepened stretches is nearly one order of magnitude higher than that of the
648 Higher Himalayan units in the klippe. Our estimates of SSP also reflect an increase by ~five
649 times within the steepened stretches.

650 **5.5. Two competing models: duplex-growth model vs. out-of-sequence fault-ramp model**

651 Deeply-incised channel morphology, steep channel gradients marked by knickpoints at
652 the upstream reaches in and around the KW could be explained by the presence of at least two
653 orogen-parallel mid-crustal ramps on the MHT (Fig.8d). Existence of two mid-crustal ramps has
654 already been shown through sequential balanced cross-sections for the last 10 Myr across the
655 Kashmir Himalaya (Gavillot et al., 2018). The study by Gavillot et al., (2018) focused on duplex

656 growth model as the balanced cross-section portrays several LH nappes stacked together (Fig.
657 8d). Translation on the MHT can impart differential uplift of the LH duplex across the two mid-
658 crustal ramps as ramps would show higher uplift/ exhumation due to higher angle of dip of floor-
659 thrust of the duplex. Here we provide more detailed information on spatial distribution of active
660 differential uplift across the KW (Fig.8a, 8d). Our field observation questions the existence of
661 multiple nappes forming a duplex (Gavillot et al., 2018) and rather favors anticlinal doming of
662 the pervasively-deformed Chail nappe, as suggested by Fuchs (1975) and Stephenson et al.,
663 (2000). We observe pronounced deformation at the core of the KW (Fig. 2d, 2e) suggesting that
664 this could be related to active faulting, crustal buckling or internal folding which maintain
665 continuous rock-uplift forcing the Chenab River to incise and maintain the steepened stretch of
666 KZ1. Gavillot et al., (2018) proposed that translation on a mid-crustal ramp of the MHT and no
667 surface-faulting is driving the uplift at the core of the KW (Fig.8d). We provide an alternative
668 explanation for the observed steep stream segment at the core of the KW. We speculate the
669 existence of a crustal fault-ramp emerging from the MHT that triggers rapid exhumation of the
670 hanging wall. In that case, out-of-sequence faulting causes high relief, steep channel gradients
671 and higher basinwide steepness indices over the ramp (Fig.7). Similar ramps have been proposed
672 on the MBT beneath the Dhauladhar Range (Thiede et al., 2017) and in the east of the NW
673 Himalaya (Caldwell et al., 2013; Mahesh et al., 2015; Stübner et al., 2018; Yadav et al., 2019).
674 Similar mid-crustal ramp (MCR-2) has been proposed for the western margin of the KW by
675 Gavillot et al., (2018). We don't have any direct field evidence of regional surface-breaking faults
676 which could be related to KZ2. However, rapid fluvial incision, increase in SSP and channel
677 steepness probably justify the existence of either a mid-crustal ramp or an out-of-sequence
678 surface-breaking fault.

679 Detailed structural mapping and morphometric analysis using high-resolution DEM
680 provide important constraints on the spatial extent of deformation. We are able to resolve the
681 high-relief Kishtwar Window and the surroundings into two major steep orogen-parallel belts/
682 zones (Fig. 5e, 8d) - one at the core of the KW could be an active high-angle fault-ramp
683 emerging from the MHT or a crustal ramp; and the other one observed along the western margin
684 of the KW could be another ramp on the MHT or a surface-breaking back-thrust evolving in
685 relationship to the growth of the LH duplex. More importantly, we demonstrate that the Kishtwar
686 Window is still growing and therefore could be the potential source of future seismic activity.

687

688 **6. Conclusions**

689

690 Our field observation and the characteristics of terrain morphology match well with the
691 spatial pattern of previously-published thermochronological data and indicate that the Kishtwar
692 Window is undergoing tectonic deformation, uplift and exhumation at present, on Late
693 Pleistocene-Holocene timescales, and in geological past since at least the late Miocene. By
694 compiling our new results and published records, we favor the following conclusions:

- 695 1. The Chenab River maintains an over-steepened bedrock channel and a low
696 channel width irrespective of lithological variations across the KW and beyond,
697 suggesting ongoing rapid fluvial incision related to active tectonic rock uplift.
- 698 2. Our field observations, morphometric analysis, and rock strength measurements
699 document that at least two of these major knickzones with steep longitudinal
700 gradients on the trunk stream are non-lithologic and are likely related to

701 differential rock uplift. The incision potential (specific stream power) in the
702 steepened stretches ~4-5 times higher than the surroundings.

703 3. The differential uplift can be explained either by slip on the multiple ramps on the
704 MHT and exhumation of the duplex floor-thrust or by a combination of slip on the
705 MHT ramp and active out-of-sequence faulting. As of now, we do not have any
706 evidence for large-scale out-of-sequence faulting.

707 4. Luminescence chronology of the transiently-stored sediments along the Chenab
708 River suggests that the valley had been overfilled by sediments of fluvio-glacial
709 origin as well as by hillslope sediment flux. Massive sediment aggradation during
710 ~130-80 kyr led to drainage re-organization and bedrock incision leaving behind
711 strath surfaces.

712 5. The late Quaternary bedrock incision rates near the western margin of the KW are
713 high 3.1-3.6 mm/yr while away from KW, the incision rates are low (< 1 mm/yr).

714 To summarize, our new study reinforces the importance of detailed field observation, and
715 morphometric analysis in understanding the neotectonic framework of the interiors of the
716 Himalaya. With additional chronological evidence from the transiently-stored sediments, we
717 showcase high rates of bedrock incision in the interior of the western Himalaya, which could
718 potentially be indicative of tectonic control on landscape evolution. However, to solve the debate
719 of ongoing duplex-growth vs. active out-of-sequence faulting, we would require more field data
720 on active structures and chronological constraints on deformation rates across potentially-active
721 structures.

722 **Appendix**

723 Additional maps, figures on morphometric analysis and luminescence dating are listed in

724 Appendix A. Data of rock strength measurements provided in Table C1. Luminescence sample
725 processing is elaborated in Appendix B.

726 **Code availability**

727 Authors used open-source codes of Topotoolbox and Topographic Analysis Kit Toolbox
728 for this study.

729 **Data availability**

730 Field data are already provided in Appendix 1. Additional data on luminescence dating
731 can be provided on request.

732 **Sample availability**

733 Samples used for luminescence dating are already mostly-destroyed, therefore it is
734 beyond sharing.

735 **Author contribution**

736 S.Dey, the first author, this work and completed the fieldwork, sample processing,
737 measurements and writing of this manuscript. R. Thiede helped in fieldwork, discussion and
738 writing of this manuscript. A. Biswas performed the initial morphometric analysis. N.Chauhan
739 helped in measurement of luminescence signal and assessment of the data. P.Chakravarti
740 performed the channel width calculations and compiled the rock strength measurements. V. Jain
741 helped in discussion and writing of the manuscript.

742 **Competing interests**

743 The authors declare that they have no conflict of interest.

744

745 **Acknowledgments**

746 This study is funded by the DST INSPIRE faculty fellowship program by the Department
747 of Science and Technology, India (grant #DST/INSPIRE/04/2017/003278), and IIT Gandhinagar
748 post-doctoral research fund (IP/IITGN/ES/SD/201718-01). Thiede is supported by German
749 Science Foundation (grant # DFG TH 1317-8 and 9). We thank M.K.Jaiswal and M.Rawat for
750 providing the elemental analysis. We thank Shambhu Das, Avi Das, Niklas Schaaf, Akashsingh
751 Rajput and Chamel Singh for their assistance during fieldwork. We also thank Soumyajit
752 Mukherjee, Rahul Kaushal and Shantamoy Guha for scientific inputs and comments on this
753 manuscript. We acknowledge A. Forte, Y. Gavillot, S. Hergarten and one anonymous reviewer
754 for their constructive and insightful reviews. We like to thank the editor R. Gloaguen and
755 associate editor A. Joshua West for their help during review process.

756

757 **References**

758 Abrahami, R., van der Beek, P., Huyghe, P., Hardwick, E., & Carcaillet, J. (2016). Decoupling of
759 long-term exhumation and short-term erosion rates in the Sikkim Himalaya. *Earth and Planetary
760 Science Letters*, 433, 76-88.

761 Bagnold, R. A. (1966). *An approach to the sediment transport problem from general physics*. US
762 government printing office.

763 Bhatia, T. R., & Bhatia, S. K. (1973). Sedimentology of the slate belt of Ramban-Banihal area,
764 Kashmir Himalaya. *Himalayan Geology*, 3, 116-134.

765 Bollinger, L., Henry, P., & Avouac, J. P. (2006). Mountain building in the Nepal Himalaya:
766 Thermal and kinematic model. *Earth and Planetary Science Letters*, 244(1-2), 58-71.

767 Bookhagen, B., & Burbank, D. W. (2006). Topography, relief, and TRMM-derived rainfall
768 variations along the Himalaya. *Geophysical Research Letters*, 33(8).

769 Bookhagen, B., Thiede, R. C., & Strecker, M. R. (2005). Late Quaternary intensified monsoon
770 phases control landscape evolution in the northwest Himalaya. *Geology*, 33(2), 149-152.

771 Bookhagen, B., Fleitmann, D., Nishiizumi, K., Strecker, M. R., & Thiede, R. C. (2006).
772 Holocene monsoonal dynamics and fluvial terrace formation in the northwest Himalaya,
773 India. *Geology*, 34(7), 601-604.

774 Burbank, D. W., Leland, J., Fielding, E., Anderson, R. S., Brozovic, N., Reid, M. R., & Duncan,
775 C. (1996). Bedrock incision, rock uplift and threshold hillslopes in the northwestern
776 Himalayas. *Nature*, 379(6565), 505.

777 Burgess, W. P., Yin, A., Dubey, C. S., Shen, Z. K., & Kelty, T. K. (2012). Holocene shortening
778 across the Main Frontal Thrust zone in the eastern Himalaya. *Earth and Planetary Science*
779 *Letters*, 357, 152-167.

780 Caldwell, W. B., Klemperer, S. L., Lawrence, J. F., and Rai, S. S., 2013, Characterizing the Main
781 Himalayan Thrust in the Garhwal Himalaya, India with receiver function CCP stacking: *Earth*
782 *and Planetary Science Letters*, v. 367, p. 15-27.

783 Colleps, C. L., Stockli, D. F., McKenzie, N. R., Webb, A. A. G., & Horton, B. K. (2019).
784 Neogene Kinematic Evolution and Exhumation of the NW India Himalaya: Zircon Geo-and
785 Thermochronometric Insights From the Fold-Thrust Belt and Foreland Basin. *Tectonics*, 38(6),
786 2059-2086.

787 DeCelles, P. G., Robinson, D. M., Quade, J., Ojha, T. P., Garzzone, C. N., Copeland, P., and
788 Upreti, B. N., 2001, Stratigraphy, structure, and tectonic evolution of the Himalayan fold-thrust
789 belt in western Nepal: *Tectonics*, v. 20, no. 4, p. 487-509.

790 Deeken, A., Thiede, R. C., Sobel, E. R., Hourigan, J. K., & Strecker, M. R. (2011).
791 Exhumational variability within the Himalaya of northwest India. *Earth Planetary Science Letters*,
792 305(1-2), 103–114. <https://doi.org/10.1016/j.epsl.2011.02.045>

793 Dey, S., Thiede, R. C., Schildgen, T. F., Wittmann, H., Bookhagen, B., Scherler, D., & Strecker,
794 M. R. (2016). Holocene internal shortening within the northwest Sub-Himalaya: Out-of-
795 sequence faulting of the Jwalamukhi Thrust, India. *Tectonics*, 35(11), 2677-2697.

796 Dey, S., Thiede, R. C., Schildgen, T. F., Wittmann, H., Bookhagen, B., Scherler, D., Jain, V., &
797 Strecker, M. R. (2016). Climate-driven sediment aggradation and incision since the late
798 Pleistocene in the NW Himalaya, India. *Earth and Planetary Science Letters*, 449, 321-331.

799 DiPietro, J. A., & Pogue, K. R. (2004). Tectonostratigraphic subdivisions of the Himalaya: A
800 view from the west. *Tectonics*, 23(5).

801 Duvall, A., Kirby, E., & Burbank, D. (2004). Tectonic and lithologic controls on bedrock
802 channel profiles and processes in coastal California. *Journal of Geophysical Research: Earth*
803 *Surface*, 109(F3).

804 Elliott, J. R., Jolivet, R., González, P. J., Avouac, J. P., Hollingsworth, J., Searle, M. P., &
805 Stevens, V. L. (2016). Himalayan megathrust geometry and relation to topography revealed by
806 the Gorkha earthquake. *Nature Geoscience*, 9(2), 174.

807 Eugster, P., Scherler, D., Thiede, R. C., Codilean, A. T., and Strecker, M. R., (2016). Rapid Last
808 Glacial Maximum deglaciation in the Indian Himalaya coeval with midlatitude glaciers: New
809 insights from ^{10}Be -dating of ice-polished bedrock surfaces in the Chandra Valley, NW
810 Himalaya: *Geophysical Research Letters*, v. 43, no. 4, p. 1589-1597.

811 Finnegan, N. J., Roe, G., Montgomery, D. R., & Hallet, B. (2005). Controls on the channel width
812 of rivers: Implications for modeling fluvial incision of bedrock. *Geology*, 33(3), 229-232.

813 Flint, J. J. (1974). Stream gradient as a function of order, magnitude, and discharge. *Water*
814 *Resources Research*, 10(5), 969-973.

815 Forte, A.M. and Whipple, K.X. (2019). The Topographic Analysis Toolkit (TAK) for
816 Topotoolbox. *Earth Surface Dynamics*, 7, 87-95.

817 Frank, W., Grasemann, B., Guntli, P. E. T. E. R., & Miller, C. (1995). Geological map of the
818 Kishtwar-Chamba-Kulu region (NW Himalayas, India). *Jahrbuch der Geologischen*
819 *Bundesanstalt*, 138(2), 299-308.

820 Fuchs, G. (1975). Contributions to the geology of the North-Western Himalayas. *Geologische*
821 *Bundesanstalt*.

822 Fuchs, G. (1981). Outline of the geology of the Himalaya. *Mitt. osterr. geol. Ges*, 74(75), 101-
823 127.

824 Gavillot, Y. G. (2014). Active tectonics of the Kashmir Himalaya (NW India) and earthquake
825 potential on folds, out-of-sequence thrusts, and duplexes.

826 Gavillot, Y., Meigs, A. J., Sousa, F. J., Stockli, D., Yule, D., & Malik, M. (2018). Late Cenozoic
827 Foreland-to-Hinterland Low-Temperature Exhumation History of the Kashmir
828 Himalaya. *Tectonics*.

829 Gavillot, Y., Meigs, A., Yule, Y., Heermance, R., Rittenour, T., Madugo, C., & Malik, M.
830 (2016). Shortening rate and Holocene surface rupture on the Riasi fault system in the Kashmir
831 Himalaya: Active thrusting within the Northwest Himalayan orogenic wedge. *Geological Society
832 of America Bulletin*, 128(7-8), 1070–1094. <https://doi.org/10.1130/B31281.1>

833 Harvey, J. E., Burbank, D. W., & Bookhagen, B. (2015). Along-strike changes in Himalayan
834 thrust geometry: Topographic and tectonic discontinuities in western Nepal. *Lithosphere*, 7(5),
835 511-518.

836 Herman, F., Copeland, P., Avouac, J.P., Bollinger, L., Mahéo, G., Le Fort, P., Rai, S., Foster, D.,
837 Pêcher, A., Stüwe, K. and Henry, P., 2010. Exhumation, crustal deformation, and thermal
838 structure of the Nepal Himalaya derived from the inversion of thermochronological and
839 thermobarometric data and modeling of the topography. *Journal of Geophysical Research: Solid
840 Earth*, 115(B6).

841 Hirschmiller, J., Grujic, D., Bookhagen, B., Coutand, I., Huyghe, P., Mugnier, J.-L., and Ojha,
842 T., 2014, What controls the growth of the Himalayan foreland fold-and-thrust belt?: *Geology*, v.
843 42, no. 3, p. 247-250.

844 Kaushal, R. K., Singh, V., Mukul, M., & Jain, V. (2017). Identification of deformation
845 variability and active structures using geomorphic markers in the Nahan salient, NW Himalaya,
846 India. *Quaternary International*, 462, 194-210.

847 Kumar, A., Lal, N., Jain, A. K., & Sorkhabi, R. B. (1995). Late Cenozoic–Quaternary thermo-
848 tectonic history of Higher Himalayan Crystalline (HHC) in Kishtwar–Padar–Zaskar region,
849 NW Himalaya: Evidence from fission-track ages. *Journal of the Geological Society of India*,
850 45(4), 375–391.

851 Kundu, B., Yadav, R. K., Bali, B. S., Chowdhury, S., & Gahalaut, V. K. (2014). Oblique
852 convergence and slip partitioning in the NW Himalaya: implications from GPS
853 measurements. *Tectonics*, 33(10), 2013-2024.

854 Lavé, J., & Avouac, J. P. (2000). Active folding of fluvial terraces across the Siwaliks Hills,
855 Himalayas of central Nepal. *Journal of Geophysical Research: Solid Earth*, 105(B3), 5735-5770.

856 Lavé, J., & Avouac, J. P. (2001). Fluvial incision and tectonic uplift across the Himalayas of
857 central Nepal. *Journal of Geophysical Research: Solid Earth*, 106(B11), 26561-26591.

858 Mahesh, P., Gupta, S., Saikia, U., and Rai, S. S., 2015, Seismotectonics and crustal stress field in
859 the Kumaon-Garhwal Himalaya: *Tectonophysics*, v. 655, p. 124-138.

860 Malik, J. N., & Mohanty, C. (2007). Active tectonic influence on the evolution of drainage and
861 landscape: geomorphic signatures from frontal and hinterland areas along the Northwestern
862 Himalaya, India. *Journal of Asian Earth Sciences*, 29(5-6), 604-618.

863 Miller, J. R. (1991). The influence of bedrock geology on knickpoint development and channel-
864 bed degradation along downcutting streams in south-central Indiana. *The Journal of*
865 *Geology*, 99(4), 591-605.

866 Mitra, G., Bhattacharyya, K., & Mukul, M. (2010). The lesser Himalayan duplex in Sikkim:
867 implications for variations in Himalayan shortening. *Journal of the Geological Society of*
868 *India*, 75(1), 289-301.

869 Montgomery, D. R., & Brandon, M. T. (2002). Topographic controls on erosion rates in
870 tectonically active mountain ranges. *Earth and Planetary Science Letters*, 201(3-4), 481-489.

871 Mukherjee S. (2015) A review on out-of-sequence deformation in the Himalaya. In: Mukherjee
872 S, Carosi R, van der Beek P, Mukherjee BK, Robinson D (Eds) *Tectonics of the*
873 *Himalaya*. Geological Society, London. Special Publications 412, 67-109.

874 Nábělek, J., Hetényi, G., Vergne, J., Sapkota, S., Kafle, B., Jiang, M., Su, H., Chen, J., & Huang,
875 B. S. (2009). Underplating in the Himalaya-Tibet collision zone revealed by the Hi-CLIMB
876 experiment. *Science*, 325(5946), 1371-1374.

877 Nadim, F., Kjekstad, O., Peduzzi, P., Herold, C., & Jaedicke, C. (2006). Global landslide and
878 avalanche hotspots. *Landslides*, 3(2), 159-173.

879 Nennwitz, M., Thiede, R. C., & Bookhagen, B. (2018). Fault activity, tectonic segmentation,
880 and deformation pattern of the western Himalaya on Ma timescales inferred from landscape
881 morphology. *Lithosphere*, 10(5), 632-640.

882 Ni, J., and M. Barazangi (1984), Seismotectonics of the Himalayan collision zone: Geometry of
883 the underthrusting Indian plate beneath the Himalaya, *J. Geophys. Res.*, 89, 1147 – 1163.

884 Powers, P. M., Lillie, R. J., & Yeats, R. S. (1998). Structure and shortening of the Kangra and
885 Dehra Dun reentrants, sub-Himalaya, India. *Geological Society of America Bulletin*, 110(8),
886 1010-1027.

887 Raiverman, V. (1983). Basin geometry, Cenozoic sedimentation and hydrocarbon prospects in
888 north western Himalaya and Indo-Gangetic plains. *Petroleum Asia Journal: Petroliferous basins*
889 of India, 6(4), 67-92.

890 Robert, X., Van Der Beek, P., Braun, J., Perry, C., Dubille, M., & Mugnier, J. L. (2009).
891 Assessing Quaternary reactivation of the Main Central thrust zone (central Nepal Himalaya):
892 New thermochronologic data and numerical modeling. *Geology*, 37(8), 731-734.

893 Robinson, D. M., & Martin, A. J. (2014). Reconstructing the Greater Indian margin: A balanced
894 cross section in central Nepal focusing on the Lesser Himalayan duplex. *Tectonics*, 33(11), 2143-
895 2168.

896 Royden, L., & Taylor Perron, J. (2013). Solutions of the stream power equation and application
897 to the evolution of river longitudinal profiles. *Journal of Geophysical Research: Earth*
898 *Surface*, 118(2), 497-518.

899 Scherler, D., Bookhagen, B., Wulf, H., Preusser, F., & Strecker, M. R. (2015). Increased late
900 Pleistocene erosion rates during fluvial aggradation in the Garhwal Himalaya, northern
901 India. *Earth and Planetary Science Letters*, 428, 255-266.

902 Schwanghart, W., & Scherler, D. (2014). TopoToolbox 2—MATLAB-based software for
903 topographic analysis and modeling in Earth surface sciences. *Earth Surface Dynamics*, 2(1), 1-7.

904 Searle, M. P., Stephenson, B., Walker, J., & Walker, C. (2007). Restoration of the Western
905 Himalaya: implications for metamorphic protoliths, thrust and normal faulting, and channel flow
906 models. *Episodes*, 30(4), 242.

907 Seeber, L., & Gornitz, V. (1983). River profiles along the Himalayan arc as indicators of active
908 tectonics. *Tectonophysics*, 92(4), 335-367.

909 Snyder, N. P., Whipple, K. X., Tucker, G. E., & Merritts, D. J. (2000). Landscape response to
910 tectonic forcing: Digital elevation model analysis of stream profiles in the Mendocino triple
911 junction region, northern California. *Geological Society of America Bulletin*, 112(8), 1250-1263.

912 Steck, A. (2003). Geology of the NW Indian Himalaya. *Eclogae Geol Helv*, 96, 147-196.

913 Stephenson, B. J., Waters, D. J., & Searle, M. P. (2000). Inverted metamorphism and the Main
914 Central Thrust: field relations and thermobarometric constraints from the Kishtwar Window, NW
915 Indian Himalaya. *Journal of Metamorphic Geology*, 18(5), 571-590.

916 Stevens, V. L., & Avouac, J. P. (2015). Interseismic coupling on the main Himalayan
917 thrust. *Geophysical Research Letters*, 42(14), 5828-5837.

918 Stübner, K., Grujic, D., Dunkl, I., Thiede, R., & Eugster, P. (2018). Pliocene episodic
919 exhumation and the significance of the Munsiri thrust in the northwestern Himalaya. *Earth and
920 Planetary Science Letters*, 481, 273-283.

921 Thakur, V. C. (Ed.). (1992). *Geology of western Himalaya (Vol. 19)*. Pergamon Press.

922 Thakur, V. C., Joshi, M., Sahoo, D., Suresh, N., Jayangondapermal, R., & Singh, A. (2014).
923 Partitioning of convergence in Northwest Sub-Himalaya: estimation of late Quaternary uplift and
924 convergence rates across the Kangra reentrant, North India. *International Journal of Earth
925 Sciences*, 103(4), 1037-1056.

926 Thiede, R., Robert, X., Stübner, K., Dey, S., & Faruhn, J. (2017). Sustained out-of-sequence
927 shortening along a tectonically active segment of the Main Boundary thrust: The Dhauladhar
928 Range in the northwestern Himalaya. *Lithosphere*, 9(5), 715-725.

929 Thiede, R. C., Bookhagen, B., Arrowsmith, J. R., Sobel, E. R., & Strecker, M. R. (2004).
930 Climatic control on rapid exhumation along the southern Himalayan Front. *Earth and Planetary
931 Science Letters*, 222(3-4), 791–806. <https://doi.org/10.1016/j.epsl.2004.03.015>

932 Turowski, J. M., Lague, D., and Hovius, N. (2009). Response of bedrock channel width to
933 tectonic forcing: Insights from a numerical model, theoretical considerations, and comparison
934 with field data. *Journal of Geophysical Research: Earth Surface*, 114(F3).

935 Vassallo, R., Mugnier, J. L., Vignon, V., Malik, M. A., Jayangondaperumal, R., Srivastava, P.,
936 and Carcaillet, J. (2015). Distribution of the late-Quaternary deformation in northwestern
937 Himalaya. *Earth and Planetary Science Letters*, 411, 241-252.

938 Wadia, D. N. (1934). The Cambrian-Trias sequence of north-western Kashmir (parts of
939 Muzaffarabad and Baramula districts). *Records of the Geological Survey of India*, 68(2), 121-
940 176.

941 Webb, A. A. G., Yin, A., Harrison, T. M., Célérier, J., Gehrels, G. E., Manning, C. E., & Grove,
942 M. (2011). Cenozoic tectonic history of the Himachal Himalaya (northwestern India) and its
943 constraints on the formation mechanism of the Himalayan orogen. *Geosphere*, 7(4), 1013-1061.

944 Wesnousky, S. G., Kumar, S., Mohindra, R., & Thakur, V. C. (1999). Uplift and convergence
945 along the Himalayan Frontal Thrust of India. *Tectonics*, 18(6), 967-976.

946 Whipple, K. X., & Tucker, G. E. (1999). Dynamics of the stream-power river incision model:
947 Implications for height limits of mountain ranges, landscape response timescales, and research
948 needs. *Journal of Geophysical Research: Solid Earth*, 104(B8), 17661-17674.

949 Whipple, K. X., DiBiase, R. A., & Crosby, B. T. (2013). Bedrock rivers. In *Treatise on*
950 *geomorphology*. Elsevier Inc..

951 Wobus, C. W., Hodges, K. V., & Whipple, K. X. (2003). Has focused denudation sustained
952 active thrusting at the Himalayan topographic front?. *Geology*, 31(10), 861-864.

953 Wobus, C., Heimsath, A., Whipple, K., & Hodges, K. (2005). Active out-of-sequence thrust
954 faulting in the central Nepalese Himalaya. *Nature*, 434(7036), 1008.

955 Wobus, C., Whipple, K. X., Kirby, E., Snyder, N., Johnson, J., Spyropolou, K., Crosby, B.,
956 Sheehan, D & Willett, S. D. (2006). Tectonics from topography: Procedures, promise, and
957 pitfalls. *Special papers-geological society of America*, 398, 55.

958 Yadav, R. K., Gahalaut, V. K., Bansal, A. K., Sati, S., Catherine, J., Gautam, P., Kumar, K., and
959 Rana, N., 2019, Strong seismic coupling underneath Garhwal–Kumaun region, NW Himalaya,
960 India: *Earth and Planetary Science Letters*, v. 506, p. 8-14.

961 Yin, A., & Harrison, T. M. (2000). Geologic evolution of the Himalayan-Tibetan orogen. *Annual*
962 *Review of Earth and Planetary Sciences*, 28(1), 211-280.

963

964 **Figure captions**

965

966 **Figure 1:** (a) An overview geological map of the western sector of the Indian Himalaya showing
967 major lithology (modified after Steck, 2003 and Gavillot et al., 2018) and existing structures
968 (Vassalo et al., 2015; Gavillot et al., 2018). The tectonic Kishtwar Window (KW) is surrounded
969 by exposure of MCT, locally known as the Kishtwar Thrust (KT), and exposes the Lesser
970 Himalayan nappes. The Lesser Himalaya forms a west-verging asymmetric anticline. Apatite
971 fission-track (AFT) ages are adapted from Kumar et al., (1995). (b) A balanced cross-section of
972 the NW Himalaya showing the general architecture of the Himalayan orogenic wedge (modified
973 after Gavillot et al., 2018). Note that, beneath the KW, Gavillot et al., (2018) proposed the
974 existence of at least two crustal ramps (MCR-1 and MCR-2) on the MHT, translation on which
975 may have resulted in 3.2-3.6 mm/yr Quaternary exhumation rates across the KW.

976 **Figure 2:** Lithological units and structural orientations observed in the Chenab valley. (a)
977 Steeply-dipping HHCS units near the western margin of the KW. (b) Highly-deformed
978 migmatites at the base of the KT. (c) Sub-vertical quartzite slabs of Chail Formation exposed in
979 the frontal horses of the LH Duplex (or, anticline). (d) Highly-deformed, sub-vertical and
980 pervasively folded and compressed quartzite layers within the core of the KW, the base of
981 stacked LH-nappes forming the hanging wall of the proposed surface-breaking fault (Fig. 8d). (e)
982 A close-up view of the folded quartzite units. (f) Steeply-dipping units of granite which formed
983 new penetrative foliation outcropping upstream from the fault-zone. (g) Further upstream from
984 the fault-zone, the bedrocks are gentler in the eastern edge of the KW.

985 **Figure 3:** Figure 3: Geomorphic features observed along the Chenab River across the KW. (a)
986 Where the Chenab River enters the KW, the major tributaries coming from the Zansar Range in
987 the north are characterized by 'U-shaped' valley suggesting repeated glacial occupancy during
988 the Quaternary. The Chenab valley is unusually wide here providing space for transient storage

989 of glacial outwash sediments. The present-day River re-incises these sedimentary fills.
990 Photograph was taken near the town of Padder (cf. Fig.1a). (b) At the core of the KW, the
991 Chenab valley is V-shaped, steep The Chenab River is steep and maintains a narrow channel
992 width. (c) Highly-elevated fluvial strath surfaces are preserved in the vicinity of the town of
993 Kishtwar Fluvial incision observed along the N-S traverse of the Chenab River. Photograph was
994 taken from south of the Kishtwar town. The Kishtwar surface (~400m high from the river) is
995 underlain by ~150-170m thick sediment cover overlying the tilted Higher Himalayan bedrock.
996 The River has incised another ~240m bedrock in this section. (d) Epigenetic gorge formed along
997 the Chenab River in its' N-S traverse through the HHCS. The town of Drabshalla is built on the
998 hillslope deposits. (e) Chenab River maintained very narrow channel (width: ~20-25 m) through
999 moderately-strong HHCS rocks, suggesting tectonic imprint on topography. (f) Formation of
1000 knickpoint at the confluence of the tributary with the trunk stream implying rapid fluvial incision
1001 of the trunk stream. (g) Three levels of strath surfaces observed below the Kishtwar surface. The
1002 strath levels are marked as T1 (~280m), T2 (~170m) and T3 (~120m). OSL dating of fluvial
1003 sediments lying above the T3 surface yield a minimum depositional age of $\sim 21.6 \pm 2.6$ ky.

1004 **Figure 4:** (a) Lithological distribution near the western margin of the KW (cf. Fig.8 for
1005 location). Luminescence sample (OSL and IRSL) locations and respective depositional ages (in
1006 kyr) are shown. Every sample except K16 and K17 are taken above strath level T1. K16 and
1007 K17 are taken from above the T3 level. Note that, the ages reported in italics are minimum age
1008 estimates. (b) A field photograph from the village Janwas, south of the town of Kishtwar,
1009 showing the aggraded sediments lying above the Higher Himalayan tilted bedrock units. (c)
1010 IRSL ages (in kyr) from the fluvio-glacial sediments and OSL age (in kyr) from the hillslope
1011 debris units suggest the valley aggradation probably started at the transition of the glacial to

1012 interglacial phase ~120-130 kyr and continued till ~80 kyr ago. (d) A close-up view (red
1013 rectangle in fig.4c) of the tilted fluvioglacial sediment layers showing alternate conglomerate and
1014 medium-coarse sand layers. (e) A ~3m thick fine sand layer within the hillslope debris yield
1015 depositional age of $\sim 86 \pm 5$ kyr. Photograph was taken near the village Pochal, northwest of the
1016 town of Kishtwar.

1017 **Figure 5:** Regional variations in (a) topography, (b) topographic relief (moving window of ~4
1018 km) (c) TRMM-derived rainfall (after Bookhagen and Burbank, 2006), and (d) Basinwide
1019 Normalized steepness indices (ksn value) of the region shown dashed box in Figure 1a. (e)
1020 Swath profiles (swath window: 50 km) along the line AB (cf. Fig.5a) demonstrate the orogen-
1021 perpendicular variations in elevation, rainfall and ksn value. KW is characterized by high
1022 elevation, high relief and high steepness, but low rainfall.

1023 **Figure 6:** Longitudinal profile of the Chenab River show major changes in channel gradient
1024 associated with knickpoints in the upstream. It illustrates the major changes in the channel
1025 gradient extend over the full length of the KW and strongest changes are located in the core and
1026 not at the margins of the window. We classified knickpoints on the basis of their genesis. The
1027 substrate lithology along the River is shown. Knickpoints caused by glacial occupancy (G1, G2
1028 and G3) are adapted from Eugster et al., (2016), who reconstructed the timing of maximum
1029 glaciation and extent of glacial cover in source region of upper Chenab River basin during the
1030 last glacial maximum. These knickpoints highlight the importance of glacial erosion in the high-
1031 elevation sectors, especially in the northern tributaries of the Chenab River. Further in this study,
1032 we focused on the area marked by red rectangle.

1033 **Figure 7:** Along-river variations in (a) channel-elevation, (b) channel width, (c) channel
1034 gradient, (d) Normalized steepness index, and (e) rock-strength of non-fractured bedrock units

1035 (R-value taken by rebound hammer) till 165 km upstream from the MBT (point X, cf. Fig.1a).
1036 The mean $R\text{-value} \pm \sigma$ for each rock type has been plotted against their spatial extent. We
1037 identified two distinct zones (K1 and K2) of high channel gradient and steepness index, which
1038 maintain low channel width despite the variable rock strength of the substrate. Knickpoint KP4
1039 may have been generated by the formation of the epigenetic gorge along the N-S traverse of the
1040 Chenab River (cf. Fig.3c). Knickpoints KP1 and KP5 mark the transition of a soft-to-hard
1041 bedrock substrate.

1042 **Figure 8:** (a) Detailed structural data from the study area showing structural and lithological
1043 variations (modified after Steck, 2003; Gavillot et al., 2018). (b) and (c) orogen-perpendicular
1044 drop of the Chenab trunk stream across stretch 1 and stretch 2, respectively, showing transient
1045 increase in steepness over the K1 and K2 knickzone. The orthogonal profile projection method
1046 has been used in the case of K2 (cf. fig.7) to identify the width of the steep segment. (d)
1047 Comparison between two deformation models explaining the observed morphometric variations
1048 across the KW – (a) duplex-growth model (adapted from Gavillot et al., 2018) and (b) active out-
1049 of-sequence fault model.

1050 **Figure 9:** A satellite image of the northern Kishtwar town showing the present-day flow-path of
1051 the Chenab River (cf. Fig.8 for location). Hillslope debris originated from the steep western
1052 margin of the KW (only made of massive white quartzites) and was deposited over fluvio-glacial
1053 and glacio-lacustrine sediments and Higher Himalaya schists bedrock exposed below in the
1054 Kishtwar valley. Massive hillslope sediment flux impeded the paleo-drainage system leaving
1055 behind the paleo-valley of the tributary, the Maru River. Our interpretation of the paleo-drainage
1056 is marked in a white dashed line. (a) A view of the Kishtwar surface from the western margin
1057 of the KW showing present-day gorge of the Chenab River and its tributary. The wind-gap

1058 (paleo-valley) of the tributary is visible. (b) Thick clay-silt deposit in the wind-gap suggests
1059 abandonment of river-flow. The OSL sample is saturated and hence only denotes the minimum
1060 age of valley abandonment/ hillslope debris flow. (c) Overview picture of the frontal horses of
1061 the LH duplex and the direction of debris flow towards the Kishtwar town. (d) Angular, poorly-
1062 sorted clasts and boulders were observed at the base of the debris flow unit near the village of
1063 Pochal, north of the Kishtwar town. The white quartzites of LH are exposed in the vicinity of the
1064 Kishtwar Town (see satellite image) – only the eastern valley flank can have collapsed in the
1065 past.

1066 **Figure 10:** (a) A topographic and geomorphic profile across the Chenab valley drawn over the
1067 Kishtwar Town. The valley aggradation by fluvio-glacial and hillslope debris sediments was
1068 succeeded by a fluvial incision which penetrated through the unconsolidated sediments of
1069 thickness ~140-150m and incised Higher Himalayan bedrock by $\sim 280 \pm 5$ m, leaving behind at
1070 least three recognizable strath surfaces with a thin late Pleistocene sediment cover. The three
1071 strath surfaces are at 280 ± 5 m (T1), ~ 170 m (T2), and $\sim 120 \pm 5$ m (T3) heights from the present-
1072 day River. We assume that the present-day bedrock gorge has been carved since the deposition
1073 of the glacio-lacustrine sediment deposits (~ 100 - 130 ky) and the hillslope debris (~ 90 - 80 ky)
1074 onto former fluvial strath surface of Higher Himalayan Bedrock. The width of the fluvial strath
1075 surface where the Kishtwar Town is located indicates that the river network had been dammed
1076 earlier too. (b) Graphical representation of mean bedrock incision rates since 80 kyr. Age
1077 constraints for T3 are shown in Fig. 4a. Based on relative heights and depositional ages of late
1078 Pleistocene deposits, we propose a minimum and a maximum bedrock incision rate of 3.1-3.5
1079 mm/y and 5.2-5.6 mm/yr, respectively. However, further downstream, the bedrock incision rates
1080 calculated from bedrock straths farther downstream from the KW range 0.7-0.8 mm/yr.

1081 **Table caption:**

1082 **Table 1:** Calculations of change in specific stream power (SSP) values across the ramp and the
1083 flat segments beneath the LH Duplex. We used a uniform discharge for SSP calculation.

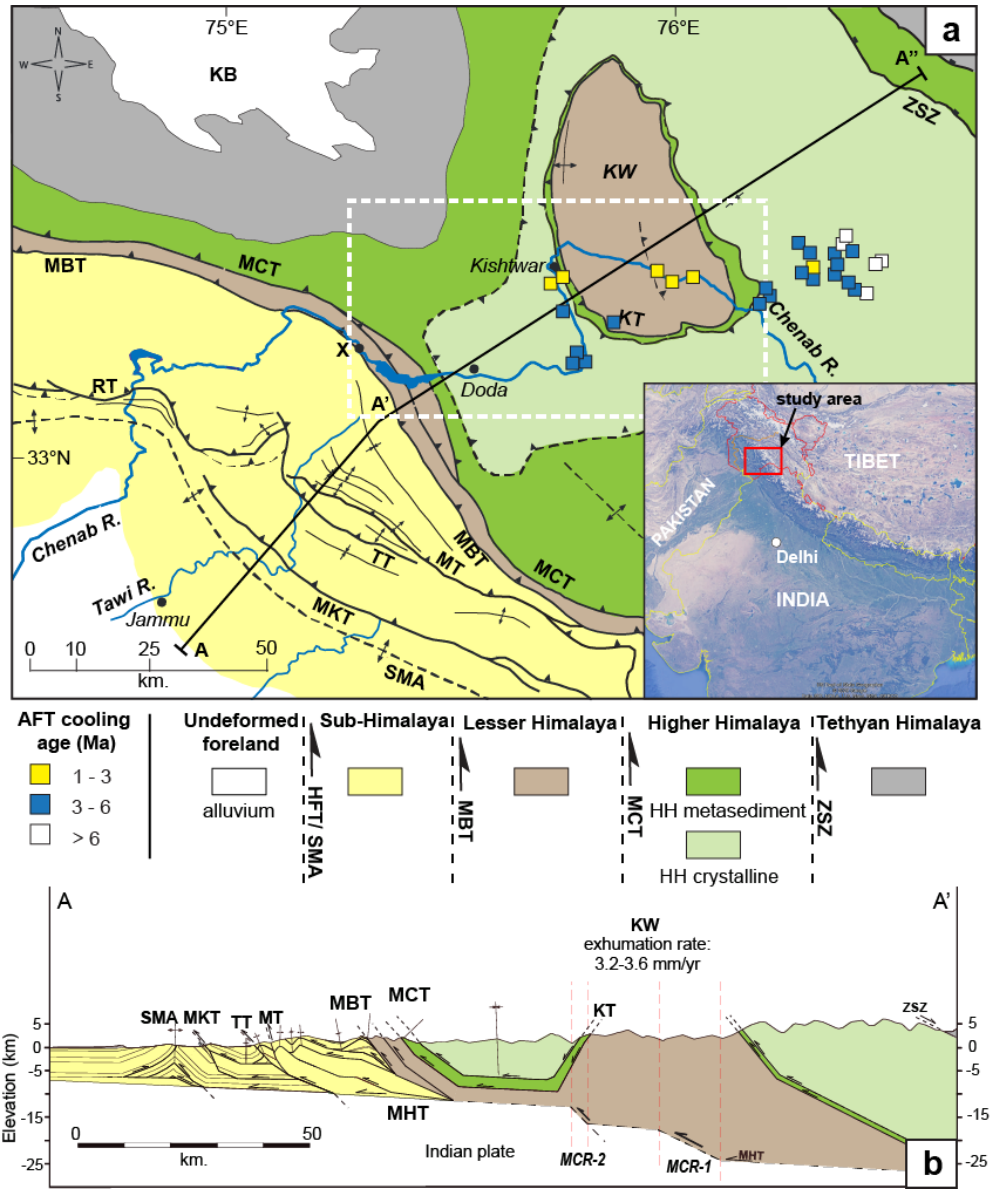
1084 **Table 2:** Sample locations, elemental concentrations, dose rates, equivalent doses and age
1085 estimations for sand samples from Kishtwar valley.

1086

1087 Figures

1088

Figure 1



1089

1090

1091

Figure 2



Figure 3

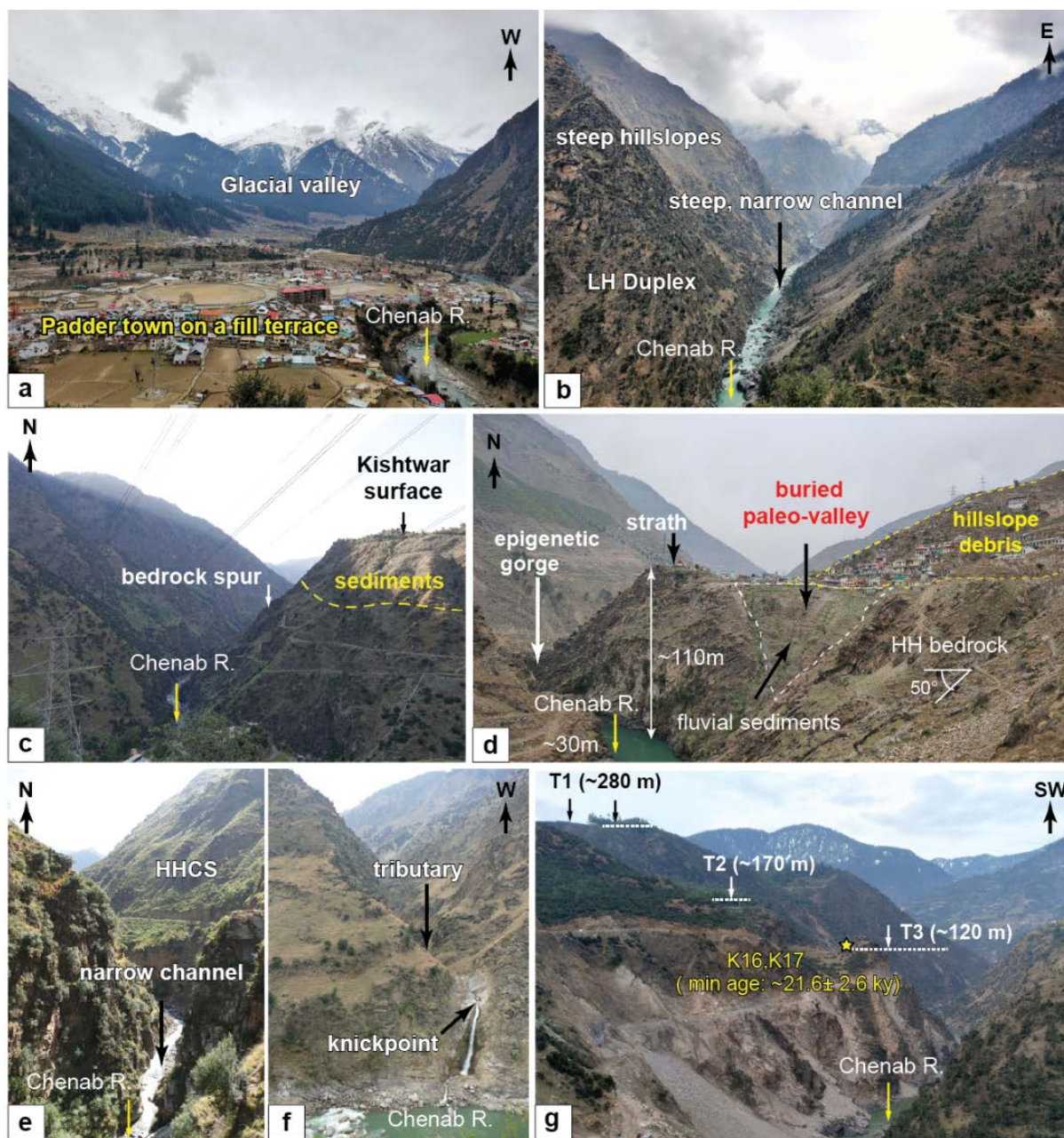
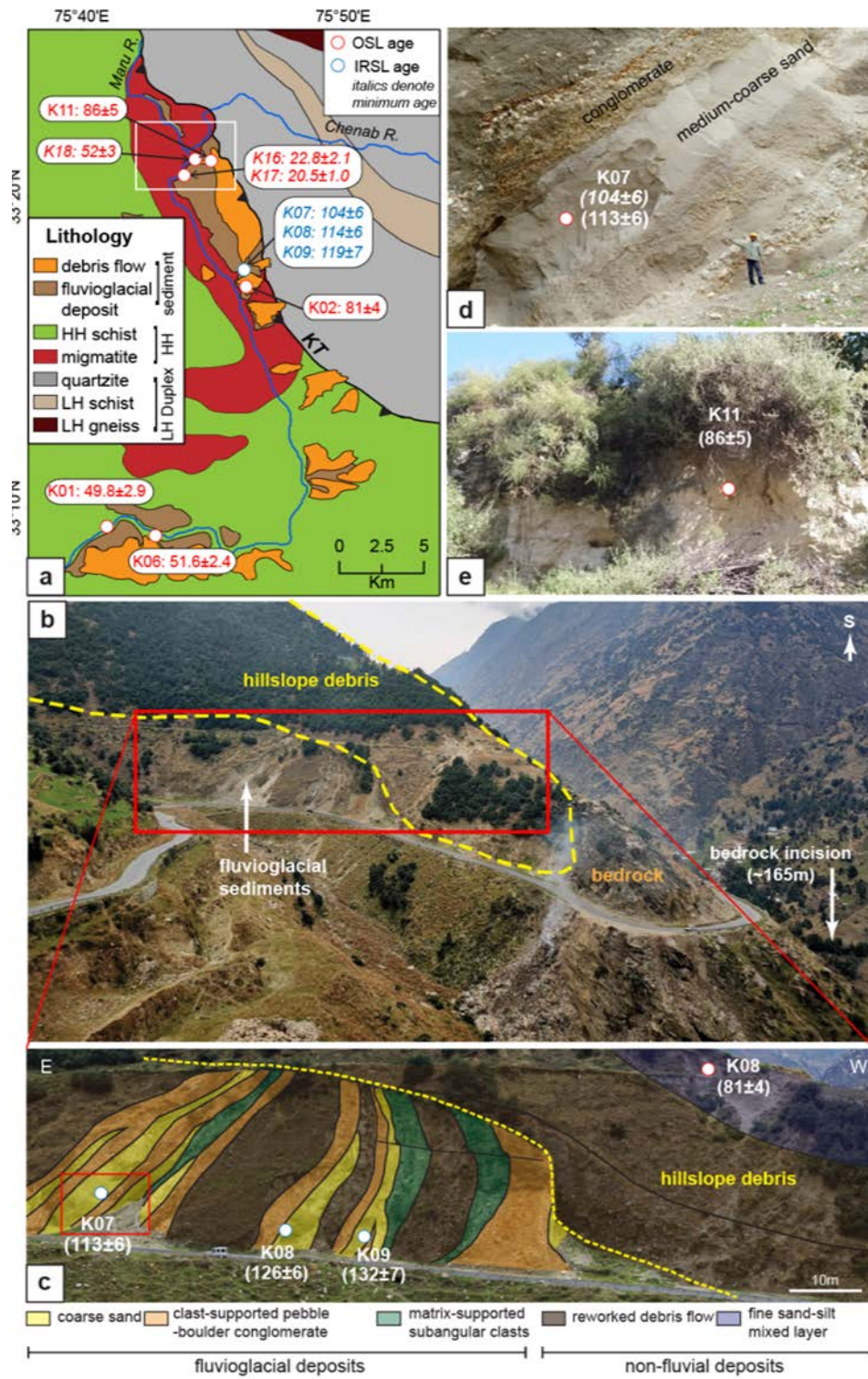
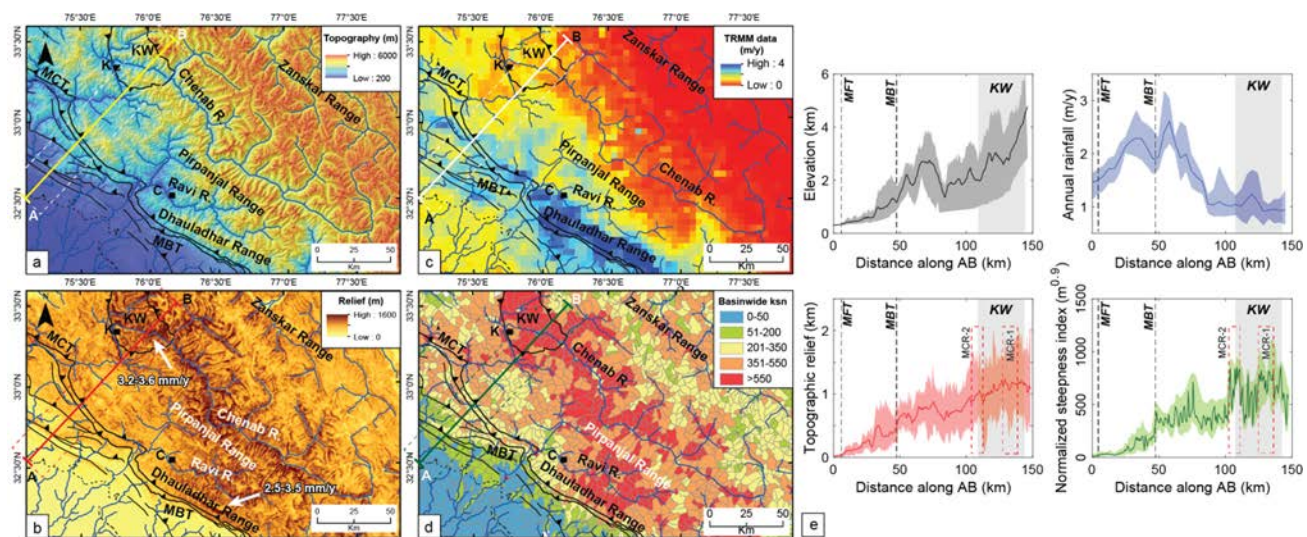


Figure 4



1101

Figure 5

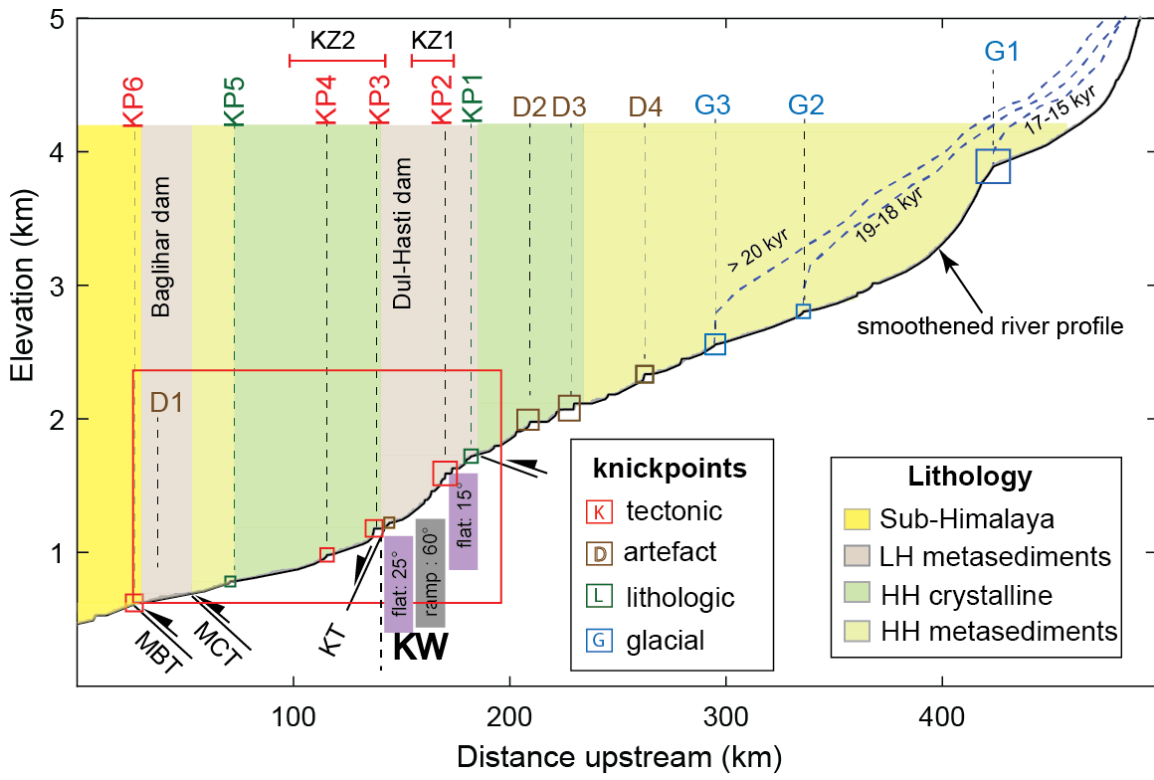


1102

1103

1104

Figure 6



1105

1106

Figure 7

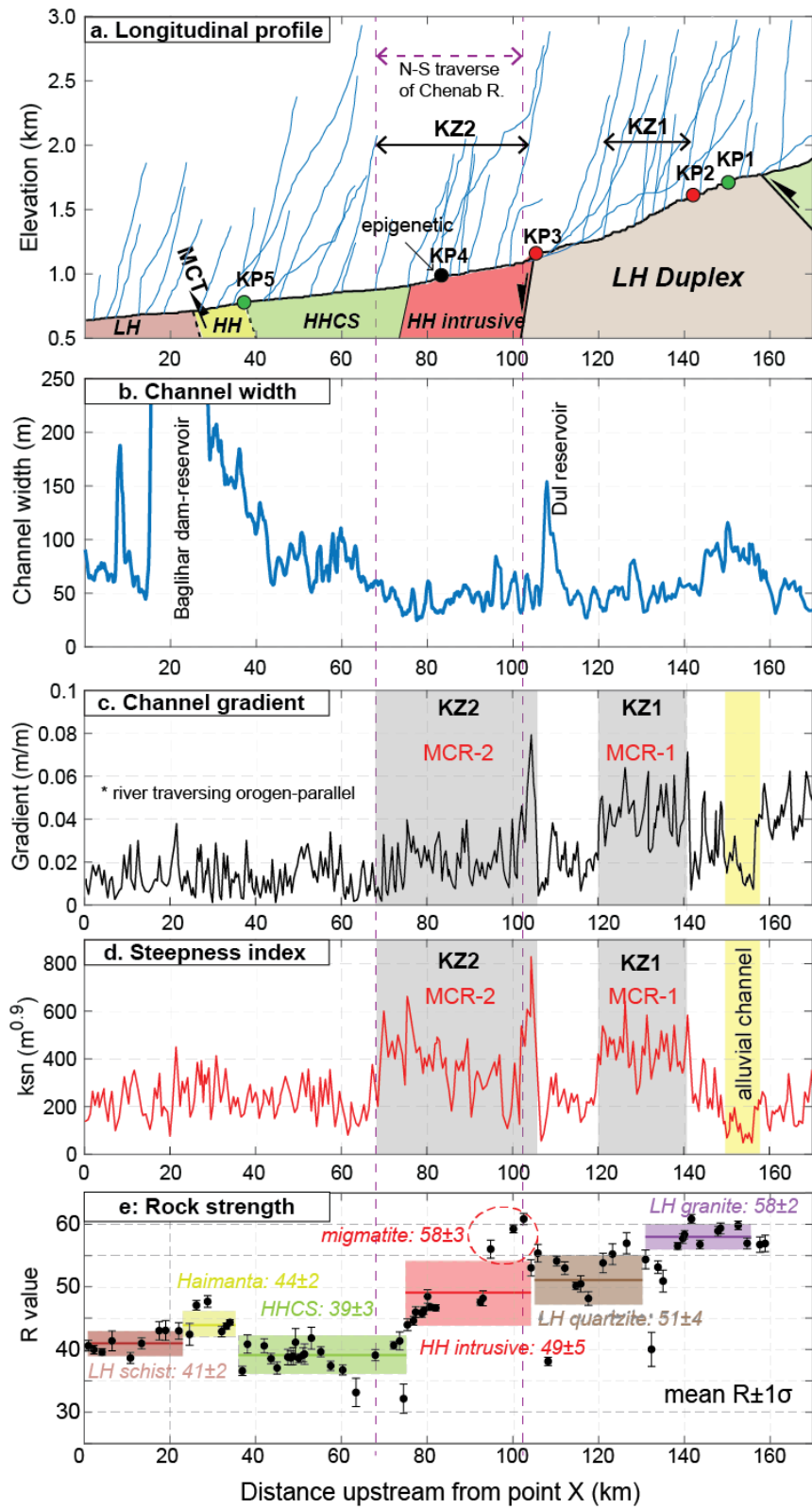
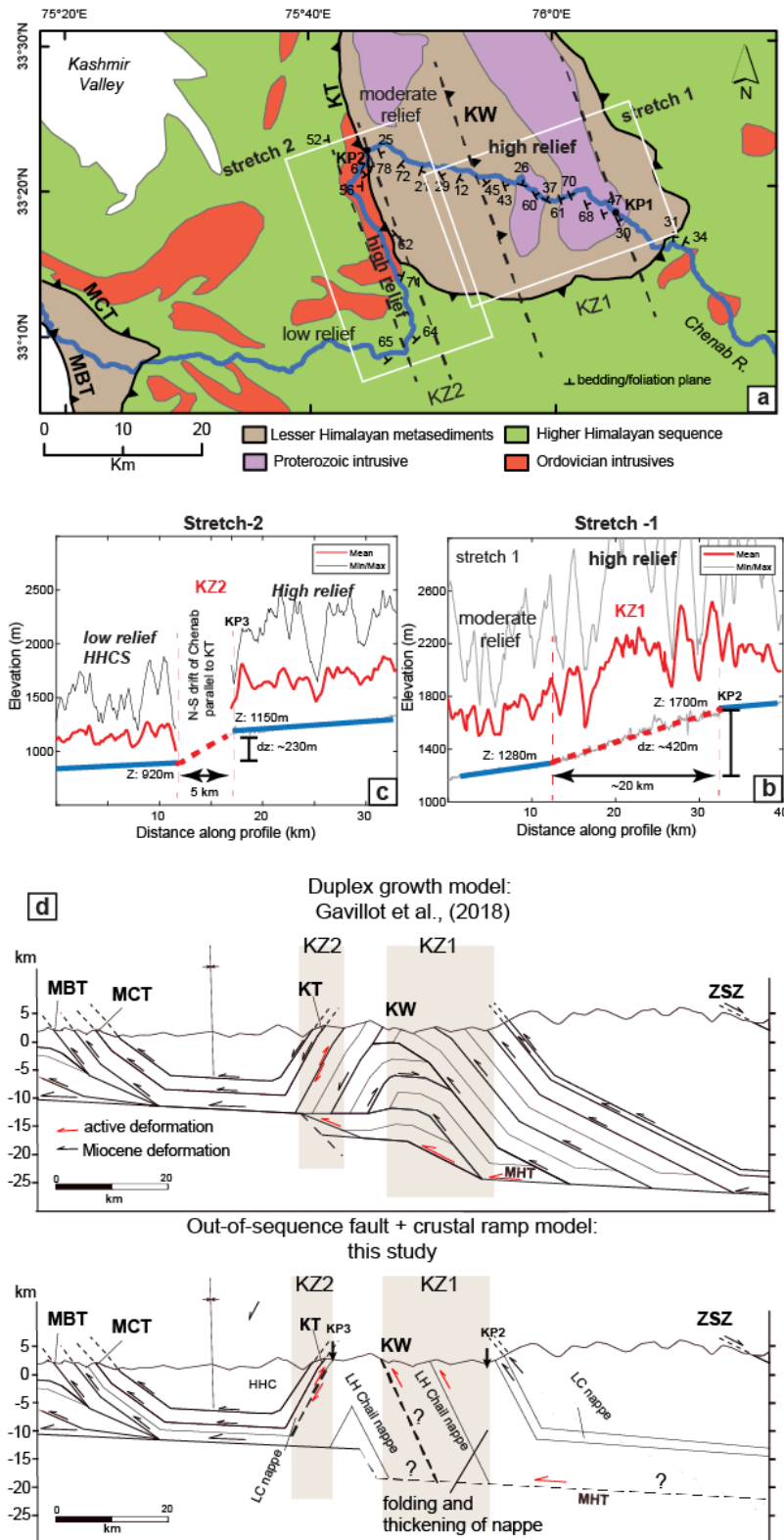
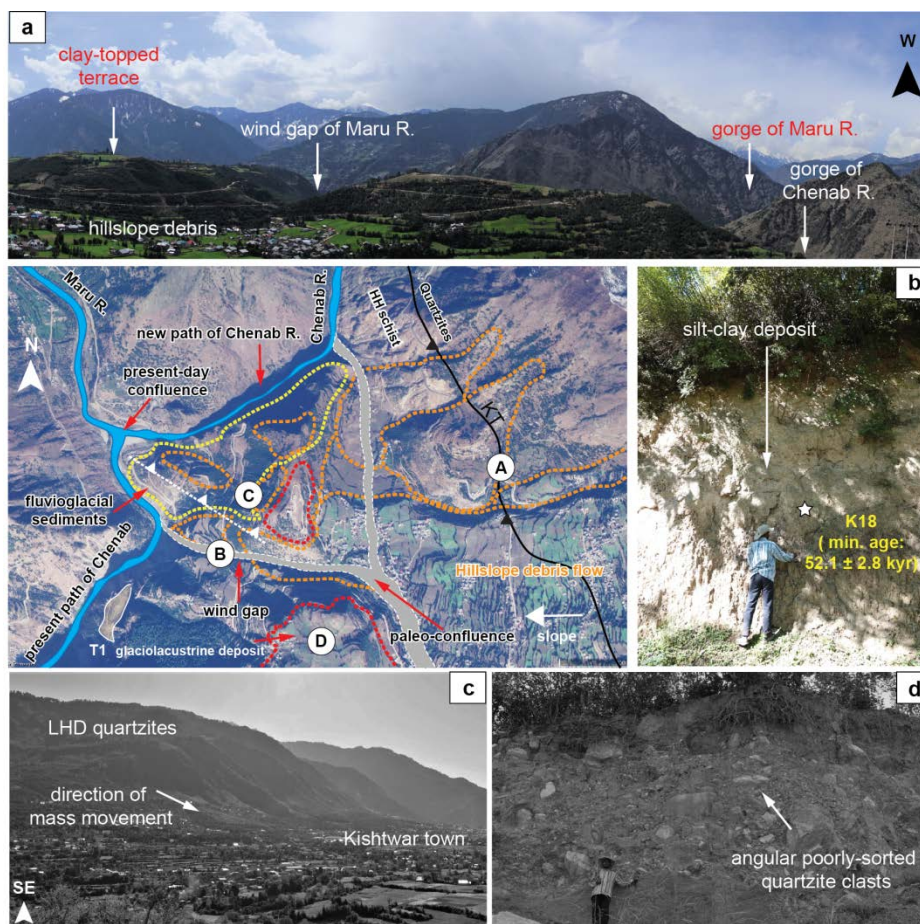


Figure 8



1113

Figure 9

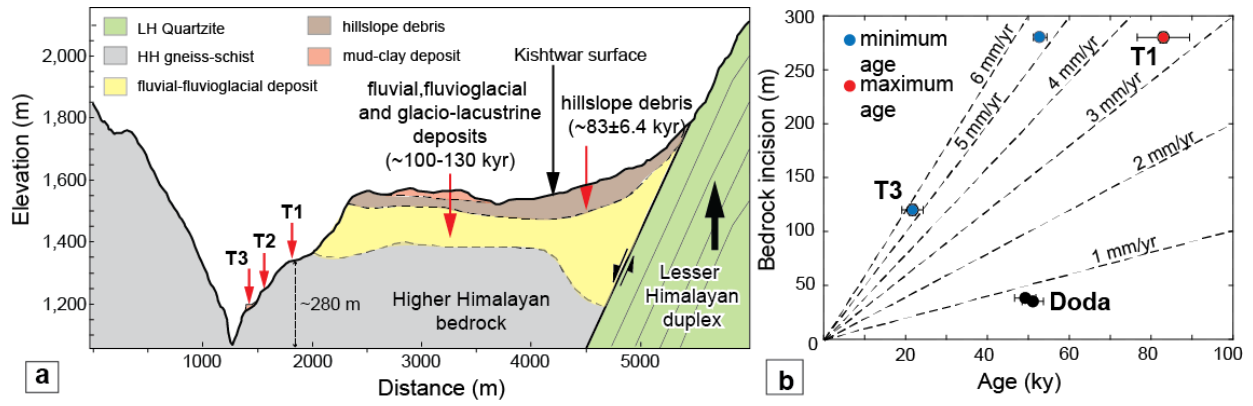


1114

1115

1116

Figure 10



1117

1118

1119

Table 1

1120

Parameter	downstream	KZ1	% change	ratio KZ1:downstream	downstream	KZ2	% change	ratio KZ2:downstream
average channel gradient (m/m)	0.006	0.021	250	3.5	0.01	0.046	360	4.6
average channel width (m)	70	45	-35.71	0.6	55	42	-24	0.76
*Specific stream power (SSP)	0.000086	0.000467	444.44	5.4	0.000182	0.001095	502	6.02

* SSP calculated by assuming equal-discharge (Q)

1121

1122

Table 2

Sample type	Sample name	Lat (°)	Long (°)	U (ppm)	Th (ppm)	K (%)	water (%)	Dose rate (Gy/ky)	De (Gy)	OD (%)	Age (ky)	fading correction	Corrected age (ky)
using central age model													
OSL	K02	33.29607	75.77619	3.8	7.2	0.46	6.1	1.74±0.02	141±8	19.5	81.1±4.6		
OSL	K11	33.35352	75.74649	3.1	12.7	2.41	6	3.97±0.09	341±19	16.8	85.7±5.1		
OSL	K01	33.15222	75.66323	2.9	13.2	2.03	9	3.88±0.04	193±11	22.1	49.8±2.9		
OSL	K06	33.15243	75.70609	3.4	18	2.17	5.4	3.97±0.05	205±10	14.4	51.6±2.4		
IRSL	K07	33.2778	75.76922	3.3	13.8	2.31	5.3	4.67±0.22	489±29	16.8	104.5±5.9	0.89	113±6
IRSL	K08	33.2778	75.76922	3.5	16.9	1.97	5.6	4.61±0.23	528±38	20.5	114.4±6.3		
IRSL	K09	33.2778	75.76922	3.3	12.2	1.98	4.8	4.29±0.20	510±42	18.1	119.2±6.8	1.11	132±7
using minimum age model													
OSL	K16	33.34873	75.73324	3.5	16.8	2.03	7.5	3.95±0.1	90±8	40	22.8±2.1		
OSL	K17	33.34873	75.73324	3.4	18	2.17	10.5	3.96±0.11	81±3.5	46	20.5±1.0		
saturated sample													
OSL	K18	33.35176	75.74325	3.3	18.7	2.61	4.5	4.36±0.13	227±14		52.1±2.8		

1123

1124

1125